A new approach for prediction of foliar dust in a coal mining region and its impacts on vegetation physiological processes using multi-source satellite datasets

Avinash Kumar Ranjan[1], Jadunandan Dash[2], and Amit Kumar Gorai[1],*

[1]Department of Mining Engineering, National Institute of Technology, Rourkela -769008, Odisha, India.

[2]School of Geography and Environmental Science, University of Southampton, Highfield, Southampton, SO17 1BJ, United Kingdom.

[3]Department of Mining Engineering, National Institute of Technology, Rourkela -769008, Odisha, India.

*Corresponding author: Amit Gorai (amit_gorai@yahoo.co.uk)

AKR (avinash.ranjan07@yahoo.com), JD (J.DASH@soton.ac.uk)

Key Points:

- Demonstrated an approach to predict foliar dust concentration from satellite data.
- Evaluated the efficacy of spectral bands of 4 satellite sensors and 26 radiometric indices.
- Quantified the effect of foliar dust on vegetation physiological processes.

Abstract

Estimating foliar dust (FD) is essential in understanding the complex interaction between FD, vegetation, and the environment. The elevated FD has a significant impacts on vegetation physiological processes. The present study aims to explore the potential of multi-sensor optical satellite datasets (e.g., Landsat-8, 9; Sentinel-2B, and PlanetScope) in conjunction with in-situ datasets for FD estimation over the Jharsuguda coal mining region in Eastern India. The efficacy of different spectral bands and various radiometric indices (RIs) was tested using linear regression models for FD estimation. Furthermore, the study attempts to quantify the impacts of FD on vegetation's physiological processes (e.g., carbon uptake, transpiration, water use efficiency, leaf temperature) through proxy datasets. The key findings of the study uncovered sensor-specific and common trends in vegetation spectral profiles under varying FD concentrations. A saturation threshold was observed around 50 g/m² of FD concentration, beyond which additional FD concentration exhibited limited impact on spectral reflectance. On the other hand, the assessment of FD estimation models revealed distinct performances and shared trends across various satellite sensors. Notably, near-infrared (NIR) and shortwave infrared-1 (SWIR1) bands, along with certain RIs, such as the Global Environmental Monitoring Index (GEMI) and the Non-Linear Index (NLI), emerged as pivotal for accurate FD estimation. Besides, the study results revealed that vegetation-associated carbon uptake experienced a ~ 2 to 3 gC reduction for every additional gram of FD per square meter. Moreover, the vegetation transpiration reduction per unit of FD ranged from approximately 0.0005 to 0.0006 mm/m²/day, highlighting a moderate impact on transpiration levels. These findings aid a significant evidence base to our understanding of FD's impact on vegetation physiological processes.

Plain Language Summary

Estimating foliar dust (FD) cover is essential to understand its impact on vegetation and the environment. Elevated FD levels can reduce photosynthesis, hinder carbon sequestration, and affect transpiration, thereby altering plant health and ecosystem functions. Accurate FD estimation helps in assessing these ecological impacts and developing strategies to mitigate adverse effects. Furthermore, FD can affect remote sensing-based analysis by altering the spectral reflectance properties of vegetation, potentially leading to inaccuracies in vegetation-related studies (e.g., health assessment, productivity estimation, species identification, etc.). By understanding these effects, the study shall aid in refining remote sensing models for more precise vegetation analysis. So, the present study utilizes multi-sensor optical satellite datasets (Landsat-8, Landsat-9, Sentinel-2B, and PlanetScope) along with in-situ data to estimate FD in the Jharsuguda coal mining region in Eastern India. Vegetation's spectral profiles under dusty and non-dusty conditions are also studied. This study also quantifies the impacts of FD on vegetation physiological processes, providing critical insights into the ecological consequences of dust accumulation on plant surfaces.

1 Introduction

Foliar dust (FD) in mining and other dusty regions negatively affects vegetation function, affecting its physiology and ecological dynamics. It affects photosynthesis, light interception, nutrient availability, gas-energy exchange, physical damage, and plant-pathogen interactions (Li et al., 2023; Naidoo and Chirkoot, 2004; Ranjan et al., 2021). The deposition of dust particles on leaf surfaces leads to obstruct stomata, the tiny openings through which plants exchange gases with the atmosphere (Li et al., 2023). This interference reduces the availability of CO_2 for photosynthesis, reduces the plant's ability to convert light energy into chemical energy, and reduces carbon assimilation and plant productivity (Chaurasia et al., 2022; Singh et al., 2023). Dust deposition on leaf surfaces negatively affects the uptake of CO_2 and the release of oxygen (O_2) through stomatal apertures (Prusty et al., 2005). The obstruction of stomata by dust limits the efficiency of gas exchange, hampering the diffusion of CO_2 into leaves and O_2 out of leaves (Chaurasia et al., 2022).

The consequences of dust deposition extend beyond photosynthesis. Dust settling on leaves and other plant surfaces hinders moisture exchange between plants and the atmosphere (Evans et al., 2019). Dust layers on vegetation leaves reduce evaporation rates and increase leaf temperature, leading to water stress and decreased transpiration (Chaurasia et al., 2022; Singh et al., 2023). This disturbance in the water cycle may reduce plant growth, especially in arid and semi-arid regions where water availability is already limited. In addition to the direct physiological effects, dust particles can cause physical damage to plant tissues (Ackerman and Finlay, 2019; Li et al., 2023). The abrasive nature of dust particles can lead to physical abrasion of leaf surfaces, epidermal layers, and cellular structures. This damage can disrupt cellular functions, alter leaf pigments, compromise plant integrity, and increase vulnerability to other environmental stresses, such as drought, heat, or pest infestations (Lin et al., 2021a; Rehman et al., 2023).

In particular, mining and roadside regions are the key hotspots of FD deposition (Kayet et al., 2019; Subpiramaniyam et al., 2021). Therefore, understanding these impacts is essential for managing and mitigating the potential ecological implications of dust deposition and ensuring the health and sustainability of vegetation ecology in these regions. However, accurate quantification and monitoring of the spatial distribution of FD deposition over large areas is a tedious and challenging task. In-situ measurement of FDC is time-consuming and labor-intensive. This makes it difficult to gather comprehensive data over large areas, as it requires substantial financial, technical, and human resources. In this context, satellite remote sensing (RS) can capture fine-scale variations, offers wide area coverage, regular monitoring, non-invasive data collection, multi-spectral capabilities, data integration, and global accessibility. Hence, integrating satellite RS data with in-situ measurements shall offer a holistic approach to FD estimation and the ability to upscale to a wider region.

So far, little attention has been given to the study of FD estimation using satellite RS, despite its significant implications for vegetation health, ecosystem dynamics, and carbon neutrality (Lin, et al., 2021b; Subpiramaniyam et al., 2021; Yu et al., 2022). Nonetheless, a study by Ma et al. (2017) focused on estimating FD in China's Changhe River mining area. Furthermore, Kayet et al. (2019) conducted a similar study over the iron ore mining region in Jharkhand state, India, using Hyperion and Landsat satellite imagery. Both studies highlighted

the importance of vegetation indices, particularly the Normalized Difference Vegetation Index (NDVI), for estimating foliar dust concentration (FDC). Apart from the mining regions, a few studies were also conducted in city or urban areas for FD mapping (Su et al., 2019; Sun et al., 2021; Yan et al., 2015; Yu et al., 2022). However, earlier studies (Kayet et al., 2019; Ma et al., 2017; Yan et al., 2015; Yu et al., 2022) have tested only a limited range of radiometric indices (RIs) (e.g., NDVI, Simple Ratio (SR), Soil Adjusted Vegetation Index (SAVI), Transformed SAVI (TSAVI), Perpendicular Vegetation Index (PVI), Non-Linear Index (NLI), Modified SR (MSR), Tasselled Cap Transformation Greenness) or relied on a single satellite sensor (e.g., Landsat, Sentinel-2) for foliar dust estimation. The potential of many other useful RIs and satellite sensor capabilities that could improve FD estimation accuracy has not yet been fully explored.

Besides the FD estimation, Ma et al. (2020) investigated the relationship between dust amount and canopy spectra in mining areas in China, and Lin et al. (2021a) examined the impact of dust deposition on pigment concentration in urban areas. In contrast, though a few past studies (Li et al., 2023; Lin et al., 2021b; Prusty et al., 2005) have discussed the negative impacts of FD deposition on vegetation biochemical properties, rarely has any study quantified its effects on vegetation physiological processes (hereafter, VPP) (e.g., carbon uptake, transpiration, leaf temperature, etc.) using satellite datasets. Long-term exposure to FD can hinder plant growth, slowing growth rates due to reduced photosynthesis, impaired gas and water exchange, increased leaf temperature, and nutrient imbalances (Chaurasia et al., 2022; Li et al., 2023; Prusty et al., 2005; Rehman et al., 2023).

Many research questions remain unanswered in the existing studies. For example, the effectiveness of different spectral bands of optical satellites, like PlanetScope, Sentinel-2, and Landsat, in estimating foliar dust concentration based on their spatial resolution, spectral characteristics, and data quality is poorly understood. Additionally, it is unclear which satellite-derived vegetation and soil radiometric indices perform best in foliar dust estimation. Moreover, the extent to which foliar dust affects vegetation photosynthesis activity, health, and productivity needs further investigation. Overall, this underexplored research area lacks comprehensive studies and methodologies, highlighting the need for further investigation. Such studies would enhance our understanding of the impacts of foliar dust on vegetation health and productivity and support effective environmental management and mitigation strategies in mining and other hotspot regions. This approach may serve as a nature-based solution (NBS) by leveraging the natural processes of plants to combat climate change while preserving ecosystem health and biodiversity. Hence, the present study aims:

(1) Characterize the spectral profile of vegetation at varying foliar dust weights using multi-sensors optical satellite datasets.
(2) Evaluating the efficacy of limited in-situ foliar dust data and different spectral bands (Landsat-8, Landsat-9, Sentinel-2, PlanetScope) and various radiometric indices for foliar dust concentration estimation in coal mining regions.
(3) Understanding the impacts of foliar dust on vegetation physiological processes (carbon uptake, transpiration, water use efficiency, leaf temperature).
(4) Investigating the role of external factors like elevation and distance from mine and roadways on FD deposition.

2 Materials and method

2.1 Study area

The present study is carried out over the coal mining region in the Jharsuguda district of Odisha state, India (**Figure 1**). The study area comes under the Mahanadi Coalfield Limited, which is a subsidiary of Coal India Limited, includes various coal mining projects, including the Belpahar opencast project (OCP), Lajkura OCP, Lilari OCP, Lakhanpur OCP, Samaleswari OCP, Hirakhand Bundia mines, and Orient Colliery U/G mines 1 and 2. The region also features other land cover types, such as forests, agricultural lands, built-up areas, and water bodies. The in-situ foliar dust samples were collected over Lakhanpur (Khairkuni region) and Samaleswari OCP, highlighted as R1 and R2, respectively, in **Figure 1** (zoomed regions).

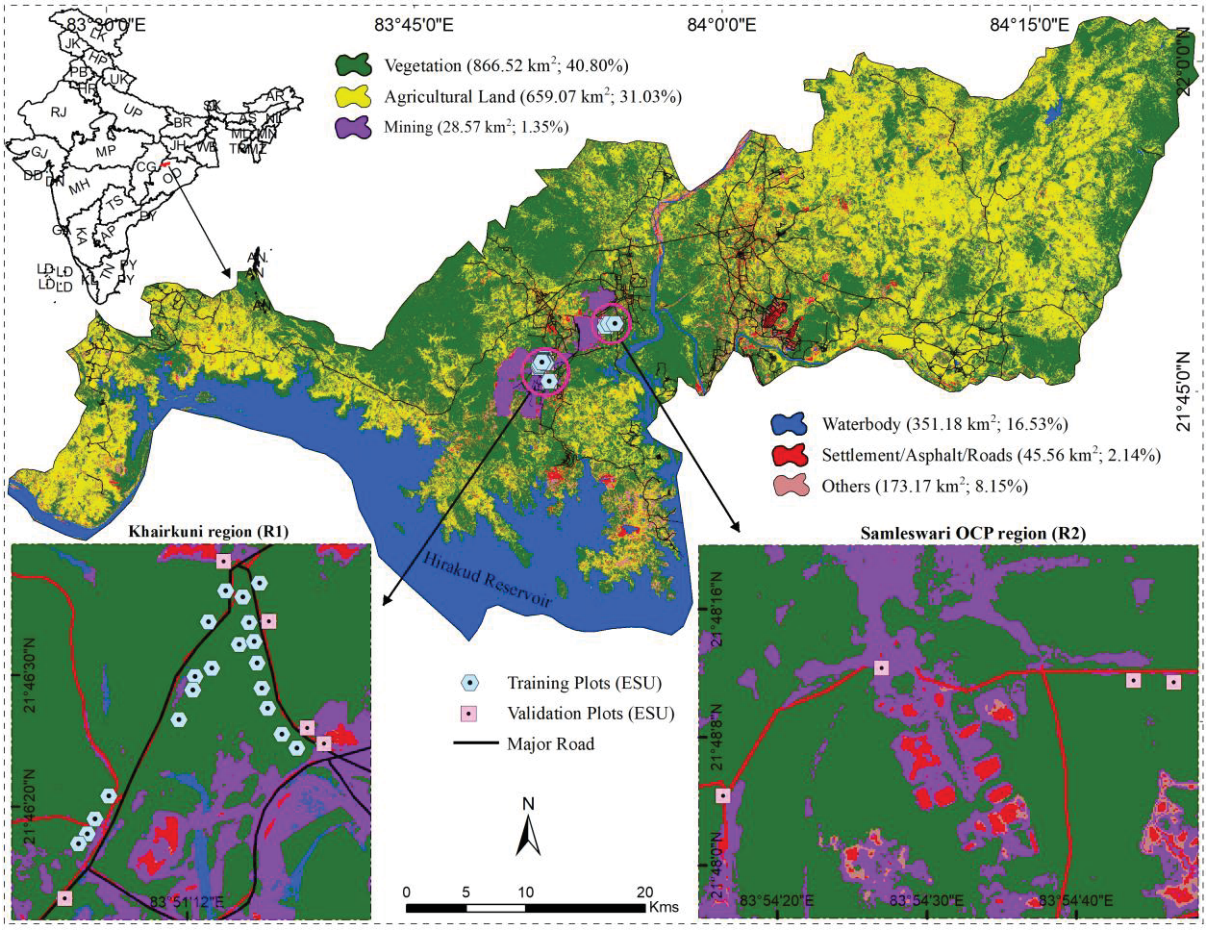

Figure 1. Location map of the Jharsuguda coal mining region in Odisha State, India. Zoomed regions highlight the sample plots for in-situ FD data collection sites.

2.2 Data

2.2.1 Multi-sensors optical satellite datasets

The present study employed four optical satellite sensor datasets (Landsat-8, Landsat-9, Sentinel-2, and PlanetScope) for FD estimations and comparative evaluation of the efficacy of different satellite sensors in FD estimations. The scenes of these satellite sensors were acquired for the nearest available date of field campaigns, as listed in **Table 1**.

The Landsat-8 and Landsat-9 surface reflectance datasets (Collection 2 Level-2 Science Products) were acquired for 13th December and 21st December 2022, respectively, from the United States Geological Survey Earth Explorer (https://earthexplorer.usgs.gov/). Both satellites offer 11 spectral bands with a spatial resolution of 30 m and a temporal resolution of 16 days. One key enhancement in Landsat-9 is the heightened radiometric resolution of 14-bit quantization from 12-bit in Landsat-8. This improvement empowers the sensors to detect subtle differences in reflectance, particularly in regions with lower radiance levels, such as bodies of water or densely vegetated forests. Band 1 to Band 7 of Landsat-8 and Landsat-9 were used in this study. Before utilizing the dataset, all the bands were converted to surface reflectance using correction factors provided in metadata files.

Sentinel-2B data with 10 m spatial resolution was also used in the study for FD estimation. Sentinel-2 offers 13 spectral bands in 10-day intervals. Sentinel-2 provides unique opportunities in the red-edge region (at 705, 740, and 783 nm), which are more sensitive and valuable in vegetation/crop-related studies. In this study, the Level-2A (S2MSI2A) atmospherically corrected SR data was acquired for 16th December 2022 from Copernicus Open Access Hub (https://scihub.copernicus.eu/dhus/#/home). Before utilizing the dataset, all the bands were resampled to 10 m.

The higher spatial resolution (3 m) data of the PlanetScope satellite was also used in the study for FD estimation and land use land cover (LULC) classification. The ortho-analytic 8-band SR (ortho_analytic_8b_sr) scenes for 14th December 2022 and 19th December 2022 were downloaded from the Planet Explorer website (https://www.planet.com/explorer/#). The PlanetScope satellite is equipped with SuperDove instruments, which capture data in 8 spectral bands (visible to NIR spectrum) daily.

2.2.2 Auxiliary satellite/gridded datasets

In this study, multiple types of datasets (satellite and ancillary) were used to investigate the impacts of FD deposition on VPP. The Moderate Resolution Imaging Spectroradiometer (MODIS)-based Gross Primary Productivity (GPP) (MOD17A2H, *v6.1*) and evapotranspiration (ET) (MOD16A2, *v6.1*) datasets were used to assess the FD impacts on vegetation carbon uptake and transpiration, respectively. The spatial and temporal resolutions of the data are 500 m and 16-day, respectively.

The GPP and ET datasets were processed and downloaded from the Google Earth Engine cloud platform (https://code.earthengine.google.com/) for the period 24th October 2022 to 19th December 2022 (dust deposition period till the field data collection). There was no rainfall in the study area from 20th October 2022 till field data collection, so it was presumed that dust started depositing on vegetation after 20th October 2022. As field visits were conducted on 14th December and 19th December 2022, the study used the mean of GPP and ET datasets (24th October 2022 – 19th December 2022), and only the best-quality pixels were considered for the study.

Additionally, the present study utilized the ECOsystem Spaceborne Thermal Radiometer Experiment on Space Station (ECOSTRESS)-based Land Surface Temperature (LST) datasets to analyze the impact of FD on vegetation temperature. ECOSTRESS mission) primarily intended to measure the plant's temperature at 70 m spatial resolution in the wavelength range 8-12.5 µm at 1-2 days intervals (https://ecostress.jpl.nasa.gov/). In the present study, atmospherically

corrected best quality Level 2 (ECO_L2G_LSTE, Version 2) datasets were acquired from NASA AppEEARS geoportal (https://appeears.earthdatacloud.nasa.gov/) for the study (date of acquisition provided in **Table 1**). A cloud bit mask band was used to screen the bad-quality data. The study used the mean of the best available LST data, corresponding to the dust deposition period.

The road network datasets were downloaded from the OpenStreetMap portal (https://www.openstreetmap.org/#map=12/21.8025/83.9033&layers=O) to investigate the relation of FDC with distance to the road. The distance to the road networks was calculated using ArcGIS software. Likely, ALOS world Digital Surface Model (DSM) based elevation data (AW3D30) was acquired from the Japan Aerospace Exploration Agency AW3D30 homepage (https://www.eorc.jaxa.jp/ALOS/en/dataset/aw3d30/aw3d30_e.htm) at 30 m resolution to examine the relation between FD and elevation.

2.2.3 In-situ data collection for foliar dust measurement

The in-situ data of foliar dust were measured for model development and validation. A total of 300 samples (dusty leaves), corresponding to 30 ESU (10 leaves from each ESU), were collected from Jharsuguda coal mining regions, as indicated in **Figure 1**. For this, the field campaigns were conducted on two different dates. The leave samples were collected from 10 elementary sampling units (ESU) in the first campaign (14th December 2022), and the same was collected from 20 ESU in the second campaign (19th December 2022). For sampling, 10 m × 10 m plots were demarcated using measuring tape and a handheld Global Positioning System (Garmin) device. The sampling plots were demarcated within relatively homogenous patches of ~ 50 m × 50 m. Due to various complexities (e.g., tree height, complex terrain, inaccessibility, etc.), sampling was restricted to limited zones. Additionally, the trees in these areas were relatively shorter, making it easier and safer to access the foliage for sampling.

The collected samples were taken to the laboratory on subsequent days for further analysis. Firstly, the weight of each dusty leaf was measured using a high-precision electronic weighing machine. Later, each dusty leaf was carefully cleaned to remove deposited dust from the leaves. The cleaned leaves were then again weighed using a high-precision electronic weighing machine. The weight of the dust concentration over each ESU was determined by comparing the dust leaf sample with the weight of the clean leaf sample (**Figure S2**). As ten leaves were collected from each site, an average of 10 leaves were considered to represent the corresponding ESU. The graph paper was used to draw the leaf area to find the dust deposition per unit area. Randomly, two leaves were taken for leaf area measurement for each ESU. Later, the average of both leaf areas was taken as the leaf area for the corresponding site. The mean dust retention of each ESU was then divided with the total leaf area to get FD deposition per unit area (g/m^2).

Table 1: *Dataset used in the present study.*

Satellite/Sensor/Data	Date of acquisition	Resolutions	Citation/Source
Landsat-8, 9	13 Dec. 2022, 21 Dec., 2022	30 m, 16-days	USGS
Sentinel-2B	16 Dec. 2022	10 m, 10 days	ESA
PlanetScope	14 Dec. 2022, 19 Dec. 2022	3 m, daily	Planet Labs
MOD17A2H, MODIS Gross Primary Productivity (GPP)	24 Oct., 1 Nov., 9 Nov., 17 Nov., 25 Nov., 3 Dec., 11 Dec., 19 Dec., 2022	250 m, 8-days	Running et al., (2015)
MOD16A2, MODIS Evapotranspiration (ET)	24 Oct., 1 Nov., 9 Nov., 17 Nov., 25 Nov., 3 Dec., 11 Dec., 19 Dec., 2022	250 m, 8-days	Running et al., (2017)
ECOSTRESS Land Surface Temperature (LST)	28 Oct., 3 Nov., 5 Nov., 9 Nov., 22 Nov., 26 Nov., 30 Nov., 4 Dec., 19 Dec., 2022	70 m, Daily	Hook and Hulley (2022)
ALOS World Digital Surface Model (DSM)	2020	30 m	Tadono et al., (2014)
Open Street Map, Roadways	-	Vector data	Open street map
In-situ Data (Foliar Dust)	14 Dec. and 19 Dec. 2022	10 m × 10 m plot	Field Visit

2.3 Method

The present study has been carried out in three parts. The first part of the study focuses on the estimation of FD using remote sensing data and associated RI of four satellite sensors and their comparative efficacies in FD estimation. The second part of the study assesses the effect of FDC on VPP. Finally, the study investigates the influence of external factors, like distance from roadways, mining, and elevation, on FD deposition. The workflow of the study is represented in **Figure 2**. The key steps of the study are discussed in the following subsections:

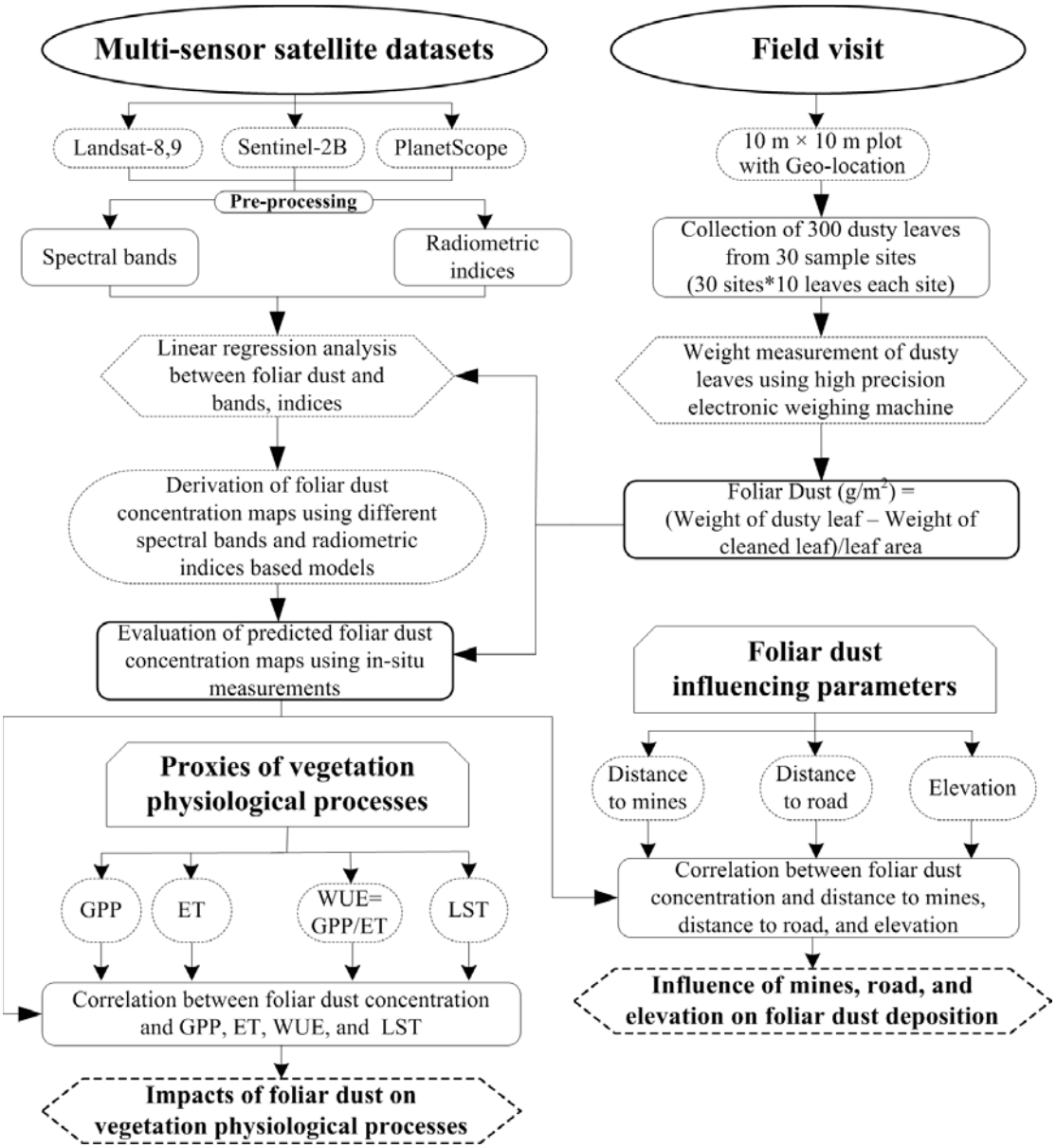

Figure 2: Flowchart showing the research methodology adopted in the study.

2.3.1 Data processing for analyses

All the satellite data (Landsat-8, Landsat-9, Sentinel-2B, and PlanetScope) were pre-processed for geometric and radiometric corrections. Subsequently, the preprocessed data were used for extracting the surface reflectance (SR) of vegetation in different dusty conditions.

Before extraction of SR data for a sampling point, the land use/land cover (LULC) of the region were studied to delineate the vegetation patches. The LULC map was broadly categorized into six classes: vegetation, agricultural land, mining, waterbody, settlement/asphalt, and others. The classification scheme of different LULC classes is provided in **Table S1**. Overall, 150 samples were taken for training, and 50 samples were taken for accuracy assessment for each class using false colour composite (FCC) images of PlanetScope data and Google Earth images. Before the accuracy assessment, manual editing of the LULC

map was also done to accurately demarcate the different spatial features, especially vegetation near the mining area, mining pits, settlements, etc. The LULC map was further used to mask other classes from the derived FD maps so that the dust concentration would be shown only for vegetation.

The spectral reflectance profiles of both dusty and non-dusty vegetation were analyzed for specified bands of four satellite sensors. This comparative analysis aimed to understand how foliar dust affects vegetation spectra under different FD weights and in dust-free conditions. Different dust weights at ~25 g/m² intervals were selected for the study. This interval was chosen based on the availability of dust samples and to provide a manageable range for analysis. For non-dusty vegetation, the mean reflectance of three-point locations was used to ensure accurate and representative values.

The satellite data were also used for deriving the radiometric indices (RIs). Eventually, the SR and RI data along with in-situ FD data were used for model development to predict the foliar dust concentration (FDC).

2.3.2 Model development for foliar dust estimation

Linear regression (LR) analysis was performed between in-situ FDC and different RIs and spectral bands to develop the FD estimation models. The current study examined the efficacy of 22 vegetation indices, 4 soil indices, and individual spectral bands of four optical satellite sensors (i.e., Landsat-8, Landsat-9, Sentinel-2, and PlanetScope) in predicting FDC. The details of all indices are provided in Supplementary **Table S2**. For the PlanetScope, an average of four pixels was used against in-situ foliar data, and single-pixel values were used for the rest of the sensors. Few RIs (e.g., Global Environmental Monitoring Index (GEMI), MERIS terrestrial chlorophyll index (MTCI), etc.) were modified by substituting the nearest bands in designated places due to non-availability of desired band data in the specific sensor. There were no specific criteria for considering/selecting RIs. Thus, all the available indices in the Sentinel Application Platform (SNAP) software were assessed in the study for ease of implementation. Any RI or spectral band-based model that exhibits significant correlation ($p = 0.01$ to 0.1) is selected for FD estimation.

2.3.3 Model performance assessment

In the present study, five commonly used statistical measures [i.e., Mean Absolute Error (MAE), Root Mean Square Error (RMSE), Percent Bias (PBIAS), and correlation coefficient (r)] were employed to assess the agreement between the satellite-based estimates and the in-situ collected FDC. In-situ FDC data of ten unused ESU were utilized for validation purposes. The MAE measures the average absolute difference between the actual and predicted values. The RMSE quantifies the average difference between the predicted values from a model and the actual observed values. PBIAS provides valuable insights into the accuracy and reliability of model predictions by quantifying the degree of systematic error or bias in the model's output compared to observed data. The r-value indicates the closeness between in-situ and predicted FDC from satellite-based models.

2.3.4 Quantifying the role of external factors on foliar dust deposition

The present study investigated the role of distance to road, distance to mining, and elevation on FD deposition through correlation analysis. The road network dataset was pooled from OSM to investigate the relation of FDC with distance to the road. Moreover, mining patches extracted from the LULC map were used to study the connection between FDC and distance to the mining patches. The distance to the road networks and distance to mining were calculated using the Euclidean function in ArcGIS software. Furthermore, DSM-based elevation data (AW3D30) was used to examine the relation between FDC and elevation. Before performing the correlation analysis, all the foliar maps were resampled to the pixel size of datasets used as proxies of VPP using the nearest neighbour function.

2.3.5 Evaluation of foliar dust impacts on vegetation physiological processes

This study used satellite-based proxies [i.e., GPP, ET, leaf temperature, and water use efficiency (WUE)] as a proxy of vegetation physiological processes (VPP) for investigations. The correlation analysis was performed between FDC and VPP proxies to understand how FD affects vegetation functions. The GPP and ET datasets were used to assess the impacts of FD on vegetation carbon uptake and vegetation transpiration, respectively. GPP data demonstrates the rate of conversion of CO_2 by vegetation into organic compounds through photosynthesis. It facilitates to analyze the changes in carbon uptake capabilities in areas with varying levels of FD deposition. Similarly, ET data, which measures the sum of evaporation and plant transpiration, helps to understand the effects of FD deposition on the water cycle within vegetation. Moreover, WUE, the ratio of carbon assimilated as biomass to water transpired by plants, was also calculated using the GPP and ET dataset (WUE = GPP/ET) to investigate its relationships with FDC. The relationship between FD and WUE helps in assessing the impacts of FD on the plant's ability to use water efficiently for atmospheric carbon assimilation in plants. Besides, the ECOSTRESS-based LST dataset was used to investigate the interplay between FD and leaf temperature. It helps in understanding the impacts of FD on vegetation's physiological status of plants and various stress conditions, including water and heat stress. Before performing the regression analysis, all the foliar maps were resampled to the pixel size of datasets used as proxies of VPP.

3 Results

3.1 Detection and delineation of vegetation zones

For detection and delineation of vegetation zones, the land use land cover (LULC) map was derived using high-resolution PlanetScope satellite data based on the Random Forest classification approach. The classified LULC map of Jharsuguda district is shown in **Figure 1**. As per the classified LULC map, vegetation covers ~ 41% (867 km^2) area of the district, followed by cropland (31%; 659 km^2), waterbody (17%; 351 km^2), others (8%; 173 km^2), settlement/asphalt (2%; 46 km^2), and mining (1%; 29 km^2). The accuracy assessment of the LULC map revealed an overall classification accuracy of ~ 94%, with a kappa coefficient of 0.92. The detailed accuracy assessment metric is provided in **Table S3**. The LULC map was further used for vegetation and mining patch extractions.

3.2 Spectral profiles of dusty and non-dusty vegetation

The results of comprehensive analyses of spectral reflectance profiles for different satellite sensors are shown in **Figure 3**. The results indicate that visible reflectance increases with low dust deposition but decreases with higher deposits for all the sensors (**Figure 3**). Specifically, the initial increase in visible reflectance is noticeable at lower dust weights (~24.33 g/m²) across all sensors. However, as dust accumulation increases (~98.05 g/m²), there is a marked decrease in visible reflectance. This trend is consistent across all sensors, indicating a uniform response to increasing dust levels. In the NIR spectrum (>700 nm), a consistent decrease in reflectance is observed with increasing dust accumulation. The NIR reflectance for non-dusty leaves is significantly higher compared to leaves with higher dust weights, and this decline becomes more pronounced as the dust weight increases, demonstrating the impact of dust on NIR reflectance. Similarly, in the SWIR spectrum (>1500 nm), initial positive reflectance changes are observed at lower dust weights (~24.33 g/m²). This positive change is more evident in the initial stages of dust deposition. However, as dust weight increases, the SWIR reflectance shows a declining trend similar to the NIR spectrum. The data from the SWIR bands indicate that dust affects not only the visible and NIR reflectance but also the SWIR reflectance characteristics.

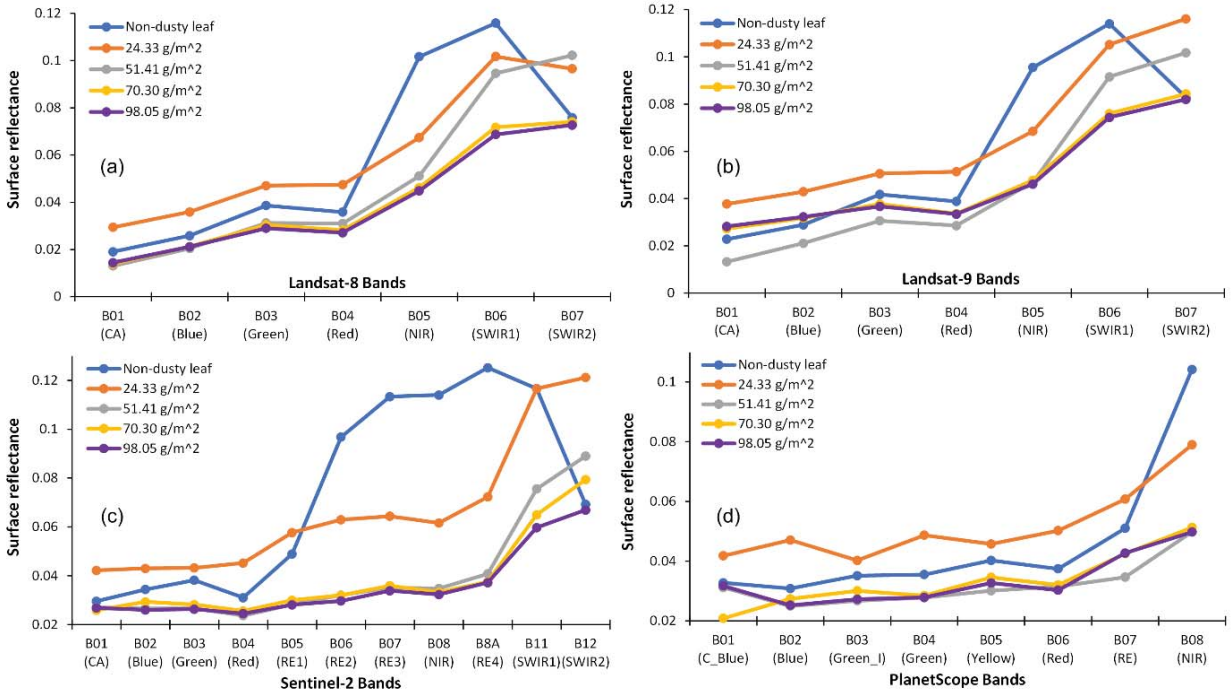

Figure 3. Spectral profile of dusty and non-dusty leaf derived from (a) Landsat-8, (b) Landsat-9, (c) Sentinel-2B, and (d) PlanetScope satellite data.

3.3 Foliar dust estimation model results

The correlation statistics (r-value) for spectral bands of different satellite sensors and RIs, based on LR models, are shown in **Figure S3.** Across all sensors, NIR bands (~865 nm) and SWIR bands (~1500-1700 nm) consistently exhibited strong negative correlations with FDC [**Figure S3 (a)-(d)**]. For PlanetScope, NIR and Red bands showed correlations of -0.661 and -0.623, respectively, aligning with the general trend of NIR and SWIR1 sensitivity to dust-induced spectral changes (**Figure 2**). Sentinel-2B displayed similar trends, with Red Edge 3 (RE3) and

narrow NIR bands showing the most pronounced negative correlations of -0.757 and -0.736, respectively. Landsat-8 also exhibited consistent trends, with the NIR band showing a correlation of -0.754 and the SWIR1 band showing a correlation of -0.645. Landsat-9 followed a similar pattern, with strong negative correlations for the NIR and SWIR1 bands. However, unexpected positive correlations were observed with the Blue (0.289) and CA (0.443) bands of Landsat-9. Further research is required to understand the factors contributing to this unexpected behaviour.

On the other hand, vegetation indices across diverse satellite platforms revealed interesting insights into their sensitivity to FDC (**Figure S3**). The correlation values of 24 RIs with FDC are summarized in supplementary **Figure S3** (**e**) **–** (**h**). PlanetScope-based GEMI showed robust negative correlation (r = -0.659) with FDC. This indicates that GEMI is more sensitive to dust-induced changes in vegetation reflectance. Similarly, other indices such as Brightness Index 2 (BI2_G_I), Non-Linear Index (NLI), and Perpendicular Vegetation Index (PVI) also exhibited significant negative correlations (r = -0.648 to -0.647) with FDC. Sentinel-2B data reaffirmed these trends, with indices like GEMIre, PVI, and Difference Vegetation Index (DVI) showing strong negative correlations. Landsat-8 data demonstrated consistent strong negative correlations with indices such as the Green Normalized Difference Vegetation Index (GNDVI), PVI, and DVI, with the Weighted Difference Vegetation Index (WDVI) displaying the highest negative correlation (r = -0.784). Landsat-9 data exhibited similar patterns to Landsat-8, with indices like WDVI, Soil Adjusted Vegetation Index 0.5 (SAVI0.5), and Modified SAVI2 (MSAVI2) showing strong negative correlations. Additionally, the Infrared Percentage Vegetation Index (IPVI) and Modified Simple Ratio (MSR) displayed notable negative correlations with dust (r = -0.775 and -0.624, respectively). This analysis offers comprehensive insights into the varied sensitivity of different spectral bands and RIs to FDC.

3.4 Performance evaluation of foliar dust estimation models

The RMSE, MAE, PBIAS, and correlation (r) were estimated to assess the accuracy and reliability of the FD prediction models. All the error metrics are summarized in supplementary **Figure S4**. From the results, it can be inferred that NIR bands and GEMI-based RI perform better in FD prediction for each sensor. For PlanetScope sensor, the blue band exhibited utmost efficacy with a correlation of 0.74 [**Figure S4** (**a**)] and a low RMSE of 22.75 g/m^2 [**Figure S4** (**m**)]. The red band also demonstrated remarkable accuracy with an RMSE of 26.25 g/m^2 and a correlation of 0.68. However, both the bands (blue and red) were incompetent at deciphering the non-dusty vegetation, as entire vegetation exhibited with FD deposition. Despite its lower accuracy metrics, the NIR band proved proficient in discriminating dusty and non-dusty leaves. RIs derived from PlanetScope data, such as GEMInir, exhibited the utmost performance with a low RMSE of 24.40 g/m^2 [**Figure S4** (**a**)] and an r-value of 0.47 [**Figure S4** (**m**)]. Similarly, the NLI exhibited competitive accuracy metrics, albeit with a tendency to slightly overestimate. In the context of Sentinel-2 data, the NIR band emerged as a key performer, standing out with a fair PBIAS [**Figure S4** (**j**)] and r-value [**Figure S4** (**n**)] despite a slightly higher RMSE [**Figure S4** (**b**)] and MAE [**Figure S4** (**f**)]. Despite its overestimation tendency, the CA band exhibited a paradoxical strong correlation with RE1. Notably, the GEMInir index stood out as a top performer among indices, with a low RMSE of 21.76 g/m^2 [**Figure S4** (**b**)]and an MAE of 19.28 g/m^2 [**Figure S4** (**f**)]. Like PlanetScope, the CA band of Sentinel-2B was also incompetent in

discriminating and deciphering the dusty and non-dusty vegetation, as the entire vegetation showed dust deposition. Notably, RE3 and RE2 bands were also observed with less RMSE [**Figure S4** (**b**)], MAE [**Figure S4** (**f**)], PBIAS [**Figure S4** (**j**)], and a strong positive correlation (r = > 0.5) [**Figure S4** (**n**)] with in-situ data. On the other hand, the Landsat-8 OLI data revealed the effectiveness of the NIR band in accurately estimating FDC, with relatively low RMSE (21.73 g/m^2) [**Figure S4** (**c**)] and MAE (19.08 g/m^2) [**Figure S4** (**g**)]. Furthermore, the GEMI-based model emerged as a top performer with the least RMSE (22.08 g/m^2) and MAE (19.11 g/m^2), making it a reliable choice for accurate FD predictions. Landsat-9-based models also showed more or less similar accuracy statistics as Landsat-8, wherein the NIR band and GEMI stand out as key performers [**Figure S4 (d), (h), (l), (p)**].

The analysis across different sensors pointed towards efficiency and reliability of NIR and SWIR bands, along with the GEMI and NLI index, as strong performers in FD mapping. Thus, the best models for each sensor (one band and one index) were subsequently used for deriving the spatial maps of FDC. As GEMI indices-based foliar maps across all four sensors were more accurate, they are shown in **Figure 4**. Moreover, the best spectral bands-based maps are presented in **Figure S5**. The outperformed linear models for FD mapping from individual spectral bands and indices-based models are provided in **Table 2**. Figure 5 shows that vegetation near and around the mining and roadways is predominantly affected by FD, as indicated by darker shades. These areas show significantly higher dust values compared to the surrounding non-dusty areas, suggesting that mining activities and vehicular movement (**Figure S1**) contribute substantially to the dust levels. Based on the derived maps, it was approximated that ~ 38 – 48 km^2 of vegetation cover in the study area is affected by dust (**Figure 4**). The dust-affected vegetation area, derived from the best one-band and one RI-based models are summarized in **Table S4.**

Table 2. *FD mapping models based on vegetation indices and individual spectral bands.*

Satellite/sensor	VI-based models	Spectral band-based models
PlanetScope	Dust (g/m^2) = -882.77(GEMInir) + 308.8	Dust (g/m^2) = -1975.9(NIR) + 183.99
Sentinel-2B	Dust (g/m^2) = -886.54(GEMInir) + 272.32	Dust (g/m^2) = -2085.2(NIR) + 152.54
Landsat-8	Dust (g/m^2) = -843.82(GEMInir) + 284.4	Dust (g/m^2) = -1876.1(NIR) + 164.68
Landsat-9	Dust (g/m^2) = -920.07(GEMInir) + 300.85	Dust (g/m^2) = -2012.1(NIR) + 170.02

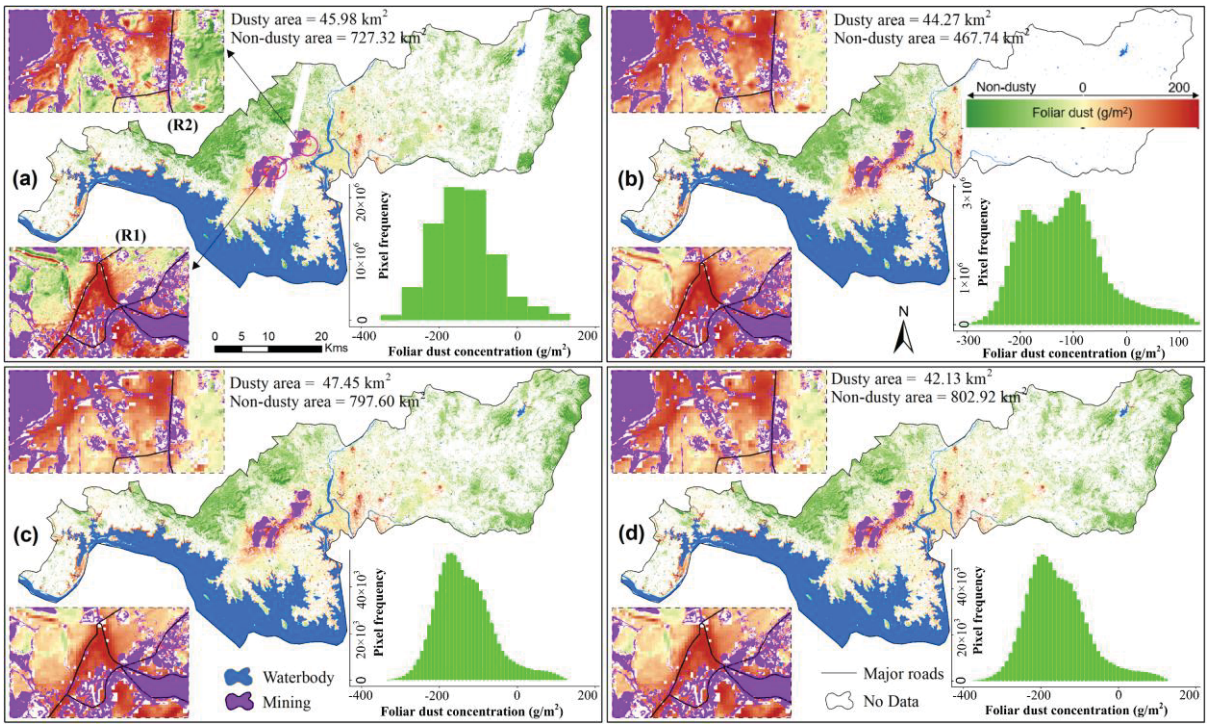

Figure 4. FD maps of the Jharsuguda district, derived using GEMI indices-based model from (a) PlanetScope, (b) Sentinel-2B, (c) Landsat-8, and (d) Landsat-9 satellite sensors**.**

3.5 Impacts of foliar dust on vegetation physiological processes

The correlation analysis between proxies of VPP and FDC, as estimated by various models, revealed notable patterns in vegetation functionality (**Figure 5**). As GEMI-indices-based foliar models were most accurate, the current analysis considered only GEMI-based estimated FD across all four sensors. The GPP, a key indicator of the total CO_2 uptake that vegetation assimilates through photosynthesis, has shown a negative correlation with FDC [**Figure 5**(**a**)]. The negative relationship, as suggested by the linear equations, indicates a decline in GPP with increasing FDC for all models. On average, the GPP loss per gram of FD deposition was approximated as 2 to 3 gC. However, the correlation between ET and FDC across different models consistently revealed a negative relationship, indicating that higher FDC are associated with reduced ET (**Figure 5b**). The magnitude of the negative correlation suggests a moderate impact of FD on ET levels. The observed reductions in ET per unit of FD range ~ 0.0005 to 0.0006 mm/m^2/day.

Additionally, the investigation into the relationship between FD and WUE across different models indicates a consistent negative impact of increasing dust concentrations on WUE [**Figure 5**(**c**)]. The analysis indicates that for every gram of FD per square meter, WUE decreases within the range of approximately 0.0121 to 0.0207 gC/kg H_2O. On the other hand, the positive correlation (r = 0.3118 to 0.4287) between FDC and leaf temperature across all models indicated a negative influence of dust deposition on the thermal conditions of vegetation [**Figure 5**(**d**)]. The positive slopes in the linear equations suggest that leaf temperature tends to rise as FDC increases. For every additional gram of FD per square meter, leaf temperature was increased by ~ 0.0376 – 0.0454 K.

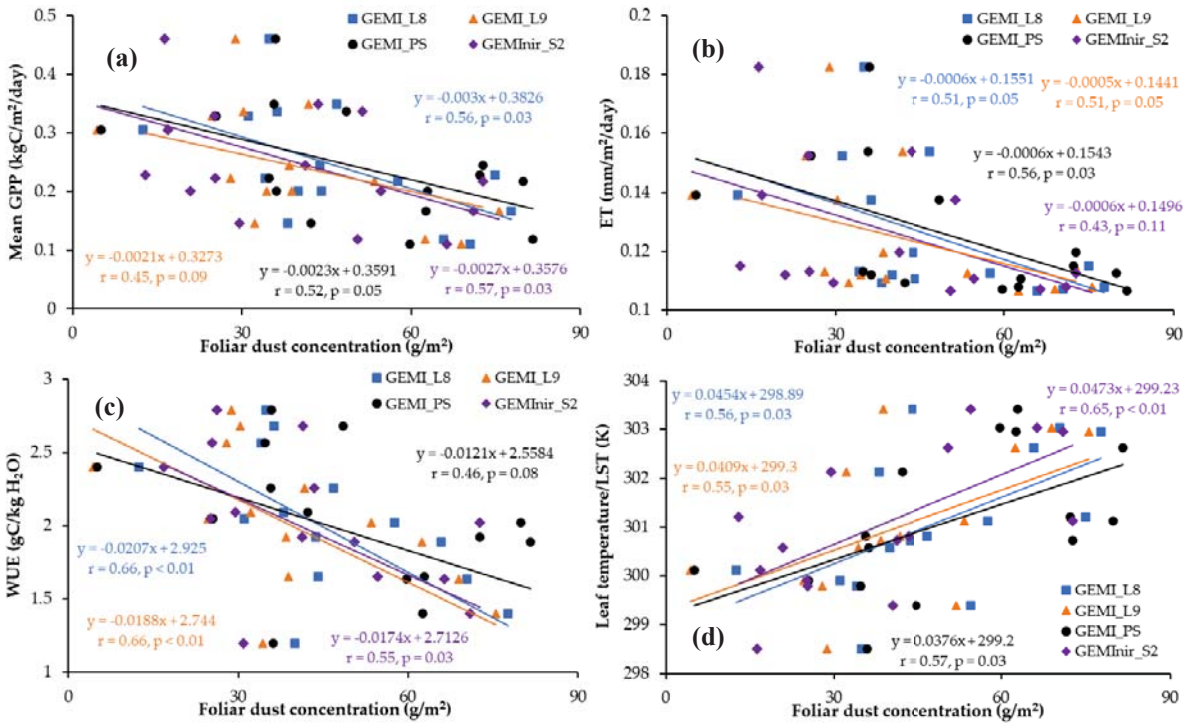

Figure 5. Association between FDC and (a) GPP, (b) ET, (c) WUE, (d) Leaf temperature**.**

3.6 Influencing parameters of foliar dust deposition

The correlation analysis between FDC predicted by various models and the distance to mines, distance to roads, and elevation revealed an inverse relationship with FD deposition (**Figure 6**). The negative correlations (r = -0.37 to -0.48) observed across all models underscore a consistent trend: FDC tends to decrease as the distance to mines increases [**Figure 6**(**a**)]. Conversely, the distance to roads revealed a similar negative correlation with FDC [**Figure 6**(**b**)]. As the distance to mines increases, the FDC tends to decrease. Besides, elevation and FD also revealed a negative correlation, indicating that FDC tends to decrease as elevation increases [**Figure 6**(**c**)]. The steeper slopes in the linear equations suggest a rapid decline in predicted FDC with increasing elevation.

However, it is important to note that not all relationships are statistically significant (up to 95% of the significance level). For instance, the p-values for the relationships between FDC and distance to mines (p = 0.07 to 0.19) and elevation (p = 0.05 to 0.08) are greater than 0.05, suggesting that these inverse relationships are not statistically significant. Only the relationship between FDC and distance to roads shows statistical significance ($p < 0.01$). These findings suggest a potential but not the definitive influence of proximity to mines and elevation on FDC compared to distance to road.

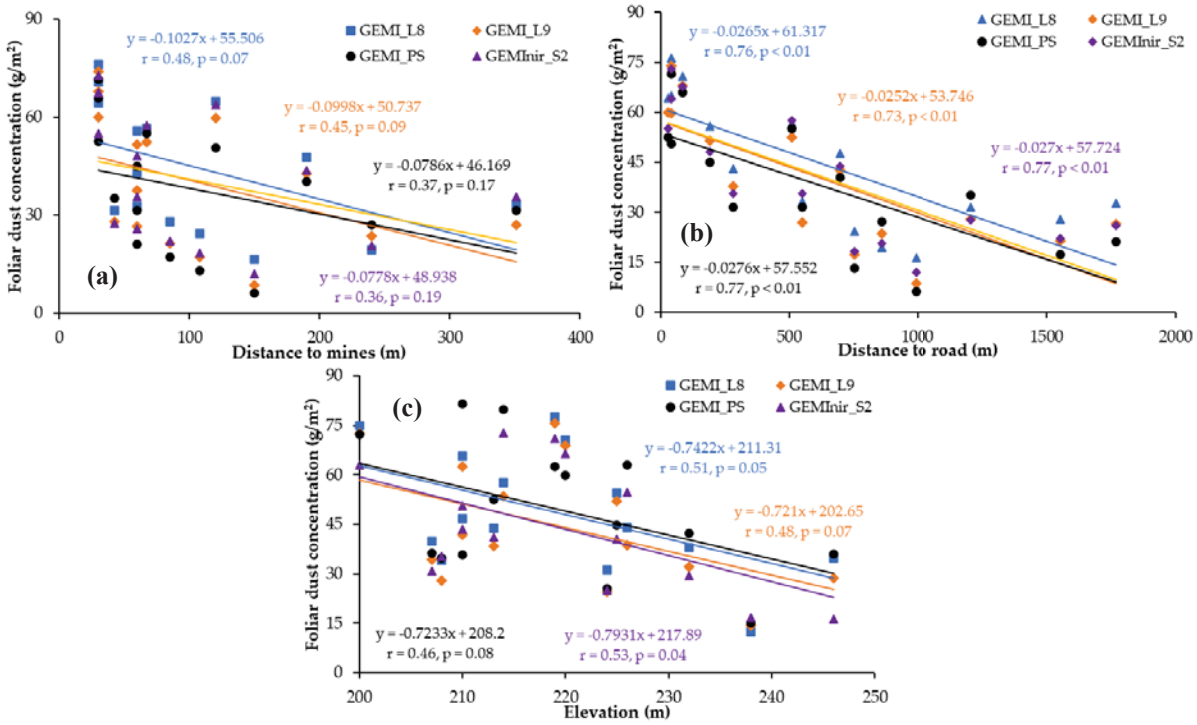

Figure 6. Relationship between FDC and (a) distance to mines, (b) distance to road, and (c) elevation**.**

4 Discussions

4.1 Spectral response of vegetation at varying foliar dust concentrations

The present study highlighted how dust deposition can significantly modify the spectral responses of vegetation, leading to deviations from the ideal spectral profile typically associated with healthy vegetation (**Figure 3**). This information on the spectral profile of dusty and non-dusty vegetation shall help to improve the accuracy of RS applications (e.g., vegetation mapping, species identification, phenology, productivity studies, etc.), monitoring vegetation health, and understanding environmental impacts. The observed deviation in the spectral reflectance (**Figure 3**) highlighted sensor-specific responses to dust-induced alterations in leaf pigments, cell structure, and water content. Consistent with a few past studies (Lin et al., 2021; Su et al., 2019; Zhou et al., 2018; Zhu et al., 2019), the present study also observed positive reflectance changes at lower dust weights, with diminishing effects at higher weights concerning the reflectance of non-dusty vegetation. The positive reflectance changes observed at lower dust weights and diminishing effects at higher weights can be attributed to optical phenomena and biological responses (Ackerman and Finlay, 2019; Zhao et al., 2020). The biological responses to dust deposition include changes in the leaf's cuticle, epidermis, and mesophyll. These alterations impact light scattering and reflectance, particularly in the NIR and SWIR spectra (**Figure S6**). FD enhances scattering effects and diffuse reflection at lower dust weights, contributing to higher reflectance values (Zhou et al., 2018). The altered orientation or structure of leaves, combined with the unique spectral characteristics of the dust, may also amplify these effects (Zhu et al., 2019). In the ideal spectral profile of vegetation (**Figure S6**), particularly in the visible spectrum (400 - 700 nm), vegetation exhibits high reflectance in the

green region (500 - 600 nm) due to the strong absorption of red and blue light by chlorophyll, resulting in the reflection of green light. This characteristic peak in green reflectance is often used as an indicator of vegetation health and vigor. Similarly, in the NIR spectrum (>700 nm), vegetation typically exhibits high reflectance due to multiple scattering within leaf tissues and the internal structure of plant cells (**Figure S6**). The consistent decrease in NIR reflectance with increasing dust accumulation observed in our study diverges from this ideal profile. This decline is possibly a result of the absorption properties of dust particles, which absorb NIR radiation rather than scattering it, leading to diminished reflectance in this wavelength range (Lin et al., 2021b). In the SWIR spectrum (>1500 nm), vegetation usually demonstrates relatively low reflectance (**Figure S6**). The observed initial positive reflectance changes at lower dust weights suggest alterations in leaf water content or surface structure, influencing the absorption and scattering of SWIR radiation. These alterations cause deviations from the typical spectral profile of vegetation in this wavelength range. As dust accumulation increases, the decline in SWIR reflectance becomes more pronounced, further highlighting the impact of dust on vegetation reflectance properties (Prusty et al., 2005).

The present study further revealed a notable saturation issue in spectral reflectance in the visible to infrared region after ~ 50 g/m² of dust accumulation across all sensors (**Figure 3**). This suggests a potential threshold beyond which additional dust fails to significantly alter reflectance across various bands, indicating the need for further investigation. However, earlier studies (Kayet et al., 2019; Ma et al., 2017; Prusty et al., 2005; Lin et al., 2021b) have not reported any saturation effects in the spectral responses of dusty leaves. This discrepancy could be due to the fact that those studies primarily derived the spectra of dusty leaves using handheld or lab-based spectroradiometers. More insights into the complex spectral behaviour of dusty and non-dusty vegetation could be gained by utilizing hyperspectral satellite sensor datasets (e.g., AVIRIS-NG, PRISMA), which provide a contiguous and large number of spectral bands. Conversely, the present study has considered one sample for specific dust weight and three samples for non-dusty vegetation, which might have also affected the observed spectral profiles. So, more sample data is required for specific dust weight to reduce the possible uncertainties and for a more confident conclusive statement. Other factors (e.g., vegetation types, fraction of vegetation cover, dust types, different pigment concentrations, leaf angle, satellite sensors angle, radiometric and spatial resolution of satellite data, etc.) could also be responsible for the observed complex spectral characteristics of dusty and non-dusty vegetation (Lin et al. 2021a; Ma et al., 2020; Su et al., 2019). So, quantifying these angles in future studies would be essential.

4.2 Foliar dust estimation: opportunities and challenges

FD mapping models across different satellite sensors revealed common and distinct performances (**Figure S4**). The consistent efficacy of NIR and SWIR bands and specific RIs, such as the GEMI and the NLI, was observed in accurate FD estimation across all the sensors (**Figure S4**). The heightened accuracy observed in NIR and SWIR bands for FD estimation can be attributed to their sensitivity to structural changes, leaf properties, and water content altered by dust accumulation (Zhou et al., 2018). NIR's strong reflection from vegetation cell structure (mesophyll) and SWIR's ability to penetrate dust layers contribute to their effectiveness (Goel and Qin, 1994; Su et al., 2019; Zhou et al., 2018). Additionally, the reduced saturation effects in

572 the NIR-SWIR spectrum (**Figure 3**) and their consistency across different sensors underline their
573 robustness in accurately discerning FD-induced alterations.
574 On the other hand, the heightened accuracy observed in GEMI and NLI indices for FD
575 mapping can be attributed to their exceptional characteristics and effectiveness. GEMI,
576 developed by Pinty and Verstraete (1991), was designed to minimize the need for detailed
577 atmospheric correction by constructing a stock atmospheric correction for the vegetation
578 index. Its formula (**Table S2**) involves multiple factors, including NIR and red bands, allowing it
579 to account for variations in atmospheric conditions. Conversely, the NLI developed based on
580 the physics of optical radiation and vegetation canopy interaction leverages multiple-angle
581 reflectance data. The indices are designed to minimize the impact of factors such as leaf angle
582 distribution, view azimuth, and soil brightness (Goel and Qin, 1994). This nuanced approach
583 enables NLI to provide robust results in complex environmental conditions, making them
584 suitable for FD mapping. In contrast, the widely used indices, like NDVI, consistently exhibited
585 higher errors and limitations in accurately predicting FDC across all sensors. Earlier studies by
586 Ma et al. (2017) and Kayet et al. (2019) have highlighted that NDVI was the best indicator for FD
587 estimation among the six tested VIs in their studies. In this context, the present study
588 contradicts the development of the NDVI-based FD estimation model due to less accuracy
589 reported in the present study.
590 The inter-comparison of satellite sensors revealed Landsat-9 as a robust performer in FD
591 estimation in the present study (**Figure S4**). Despite its coarser spatial resolution of 30 m,
592 possibly Landsat-9's advanced radiometric capabilities (14 bits), coupled with effective
593 atmospheric correction, contributed to its remarkable performance in accurate FD estimation.
594 While PlanetScope and Sentinel-2 offer finer spatial resolutions, Landsat-9 compensates for this
595 with its 14-bit radiometric resolution, allowing for enhanced detection of subtle spectral
596 differences associated with foliar dust. On the other hand, though Landsat's 30 m resolution
597 might not perfectly match the scale of the 10 x 10 m sample plots, the spatial averaging effects
598 and assumed homogeneity within the plots enabled meaningful comparisons and accurate
599 assessments of FDC at a larger scale (Ma et al., 2022; Mu et al., 2015). This comparative analysis
600 emphasizes that while spatial resolution is important, the overall technical capabilities of a
601 sensor, including radiometric resolution and atmospheric correction, play a critical role in the
602 accurate estimation of foliar dust.
603 Nevertheless, FD estimation using satellite data has several challenges. Spectral mixing,
604 caused by the combined spectral responses of dust and vegetation, can make accurate
605 quantification of dust deposition challenging, especially in cases of low dust loads or complex
606 vegetation types. In-situ data collection poses a significant challenge (e.g., tree height,
607 unfavourable landscape, etc.), requiring extensive fieldwork and reliable ground truth data to
608 improve the model's accuracy and reliability. Furthermore, the need for different models for
609 various plant species highlights the challenge of model generalization across different
610 vegetation types. These challenges underscore the importance of continued research in
611 improving the accuracy and reliability of FD estimation models.
612
613 **4.3 Nexus between foliar dust and vegetation physiological processes**
614 The present study, possibly for the first time, investigated the complex relationship between FD
615 deposition and VPP using multi-source and multi-sensor satellite datasets. It was evident in the

present study that vegetation experienced a GPP reduction ranging from 2 to 3 gC for every additional gram of dust per square meter, depending on the specific model used for FD estimation. These findings suggested that elevated FDC potentially limits the vegetation's ability to perform optimal photosynthesis and affects the ecosystem's overall carbon uptake. Moreover, the reduction in ET was observed due to increasing dust concentration, which can be attributed to several potential factors. One possible explanation is that FD deposition on vegetation surfaces may affect stomatal conductance, reducing water loss through transpiration (Chaurasia et al., 2022; Ranjan et al., 2023). Furthermore, the negative correlation between FD accumulation and WUE can be attributed to several factors. Firstly, FD deposition on plant surfaces can hinder the photosynthetic process by reducing the amount of sunlight reaching the chloroplasts. Dust particles on leaves may act as a barrier (**Figure S7**), limiting the absorption of solar radiation crucial for photosynthesis, thereby affecting the overall efficiency of carbon assimilation (Naidoo and Chirkoot, 2004). Secondly, FD can influence stomatal conductance, which is pivotal in regulating water vapor and gas exchange during photosynthesis (Zhu et al., 2019). So, the reduction in transpiration could contribute to an observed decrease in WUE. While these are general explanations, the mechanisms driving the negative correlation may vary based on environmental conditions, plant species, and the nature of dust particles. Consequently, further studies, including controlled experiments and field observations, would be instrumental in understanding the complex relationships between FD and WUE/transpiration.

On the other hand, a positive correlation between FD and leaf temperature was evident [**Figure 5 (d)**]. Dust on leaf surfaces alters the reflective properties of leaves, potentially enhancing the absorption of solar radiation and leading to an increase in leaf temperature. Moreover, dust particles, particularly darker ones, tend to absorb more sunlight, contributing to elevated temperatures (Evans et al., 2019). Dust layers may create a thermal barrier, limiting heat dissipation from the leaf and increasing temperature (Evans et al., 2019). Besides, it is essential to emphasize that correlation does not imply comprehensive causation, and the observed relationship needs further investigation. Controlled experiments and detailed field studies would be valuable for elucidating the specific mechanisms through which FD deposition influences leaf temperature.

4.4 Influencing parameters of foliar dust

The present study demonstrated that distance to roads is a more influential factor in FD deposition compared to elevation and distance to mines, as indicated by a stronger and more significant negative relationship with FDC (**Figure 6**). However, not all relationships were statistically significant (up to $p \leq 0.05$), particularly in the case of distance to mines and elevation. The unpaved nature of these roads, coupled with intense vehicular traffic associated with mineral transport, contributes to increased dust emissions and subsequent deposition on vegetation (Prusty et al., 2005). The constant movement of trucks and other vehicles on unpaved surfaces disturbs the soil, leading to increased dust emissions [**Figure S1 (e)**]. On the other hand, the fair and negative correlation between FD and elevation could include the impact of topography on wind patterns. Higher elevations may result in increased wind speed (Yu et al., 2013), leading to better dispersion of dust particles. The elevation is often correlated with changes in temperature and humidity (Rangwala and Miller, 2012), which can impact the

settling and retention of dust particles on foliage. At higher elevations, cooler temperatures can lead to increased air density and reduced turbulence, facilitating dust particles settling onto foliage (Zender et al., 2004). Additionally, variations in humidity affect the stickiness of leaf surfaces; higher humidity can create moisture films on leaves, enhancing the adhesion and retention of dust particles. Conversely, lower humidity can result in drier leaf surfaces, making it more difficult for dust to adhere (Pöschl, 2005). Furthermore, shorter vegetation, often found in areas affected by vehicular movement, is more likely to accumulate dust due to its proximity to the ground, where dust is generated and quickly settles. Therefore, changes in temperature, humidity, and vegetation height associated with elevation play a crucial role in the settling and retention of dust particles on vegetation.

Nevertheless, it is also essential to note that numerous other factors, such as climatological factors (e.g., wind speed, wind direction, humidity, etc.), geological factors (e.g., dust composition), vegetation characteristics (e.g., tree height, leaf texture), etc., may also have a substantial impact on FD deposition. For instance, wind speed and direction influence the transport and distribution of dust particles, potentially increasing or decreasing deposition rates depending on the terrain and vegetation cover (Beckett et al., 2000; Zender et al., 2004). Humidity affects how dust particles adhere to leaf surfaces, with higher humidity enhancing adhesion due to the formation of moisture films (Pöschl, 2005; Wang et al., 2013). Geological factors like dust composition can determine the size and weight of dust particles, influencing their ability to settle on vegetation (Goudie and Middleton, 2006; Ranjan et al., 2022). Vegetation characteristics such as tree height, leaf area, leaf texture, etc. can also affect how much dust is captured and retained, with shorter vegetation and rougher leaf surfaces generally accumulating more dust (Linden et al., 2023; Song et al., 2015). Due to certain limitations, including the coarser spatial resolution and the unavailability of specific datasets, examining these additional factor's influence on vegetation FDC was not feasible within the scope of this research.

5 Conclusions

The present study unveiled opportunities and challenges in accurate FD estimation. Furthermore, this study revealed the multifaceted consequences of dust deposition on crucial ecological processes. Based on the present study, the following conclusions are drawn:

1. The study revealed the complex spectral responses of vegetation to varying FD. A saturation threshold emerged near ~ 50 g/m² dust concentration, beyond which additional FD exhibited limited impact on spectral reflectance across various bands.
2. The enhanced efficacy of FD estimation models varied, with NIR & SWIR1 bands and GEMI & NLI indices across the sensors, while commonly used NDVI exhibited limitations.
3. The Landsat-9 sensor outperformed other sensors' accuracy and reliability in FD estimation, potentially due to its improved radiometric resolution (14 bits) capabilities.
4. Proximity to distance to roads and elevation were identified as key factors influencing FD deposition.
5. The research unveiled negative correlations between FD and GPP, ET, and WUE, indicating potential reductions in photosynthesis, carbon uptake, transpiration, and water use efficiency with increasing dust levels.

6. Positive correlations between FD and leaf temperature suggested a potential influence of dust deposition on the thermal conditions of vegetation.

This comprehensive study significantly aids our understanding of FD's intricate influence on vegetation. The complex insights into FD estimation models, spectral behaviors, and vegetation functionality provide a solid foundation for informed environmental management. It further highlights the need for ongoing research to address challenges and refine methodologies to comprehend and mitigate the impacts of FD on ecosystems.

Acknowledgments

The author would also like to thank the United States Geological Survey (USGS) and the European Space Agency (ESA) for Landsat-8,9, and Sentinel-2B data. The authors sincerely acknowledge the mission scientists and principal investigators of MODIS satellite products (i.e., MOD17A2H, MOD16A2), ECOSTRESS Land Surface Temperature data, ALOS World Digital Surface Model data, and Open Street Map (OSM), who provided the data used in this research effort. The author sincerely acknowledges Planet Labs for providing access to PlanetScope imagery. Google Earth Engine (GEE) and NASA Appears are also sincerely acknowledged for providing the cloud/web-based platform. AKR is thankful to M. K Swain, P. Behera, G. Srikanth, Arjun, Pratap Kumar, Deptanshu, and others for helping in field data collection and laboratory experiments. Department of Biotechnology and Medical Engineering, NITRKL, is sincerely acknowledged for providing the confocal microscope instrument for the experiment. The authors extend their gratitude to the anonymous reviewers for their valuable suggestions, which have significantly improved the overall quality of the manuscript.

Data Availability Statement

The data on which this article is based are available in the following referenced works and sources: Landsat-8, 9 data are available from the USGS (https://earthexplorer.usgs.gov/); Sentinel-2B data are available from the ESA Copernicus Data Space Ecosystem (https://tinyurl.com/28vtapuj); PlanetScope data are available from Planet Labs (https://www.planet.com/explorer/#); MOD17A2H (MODIS GPP) data are available from Running et al. (2015); MOD16A2 (MODIS ET) data are available from Running et al. (2017); ECOSTRESS LST data are available from Hook and Hulley (2022); ALOS World DSM data are available from Tadono et al. (2014); Roadways data are available from Open Street Map (https://www.openstreetmap.org/); Foliar Dust data were collected during field visits on 14 and 19 December 2022, and can be provided upon reasonable request.

References

Ackerman, D. E., & Finlay, J. C. (2019). Road dust biases NDVI and alters edaphic properties in Alaskan arctic tundra. Scientific Reports, 9(1), 214. https://doi.org/10.1038/s41598-018-36804-3

Beckett, K. P., Freer-Smith, P. H., & Taylor, G. (2000). Particulate pollution capture by urban trees: effect of species and windspeed. Global change biology, 6(8), 995-1003. https://doi.org/10.1046/j.1365-2486.2000.00376.x

Chaurasia, M., Patel, K., Tripathi, I., & Rao, K. S. (2022). Impact of dust accumulation on the physiological functioning of selected herbaceous plants of Delhi, India. Environmental

747 Science and Pollution Research, 29(53), 80739–80754. https://doi.org/10.1007/s11356-
748 022-21484-4
749 Evans, S., Malyshev, S., Ginoux, P., & Shevliakova, E. (2019). The Impacts of the Dust Radiative
750 Effect on Vegetation Growth in the Sahel. Global Biogeochemical Cycles, 33(12), 1582–
751 1593. https://doi.org/10.1029/2018GB006128
752 Goel, N. S., & Qin, W. (1994). Influences of canopy architecture on relationships between
753 various vegetation indices and LAI and Fpar: A computer simulation. Remote Sensing
754 Reviews, 10(4), 309–347. https://doi.org/10.1080/02757259409532252
755 Goudie, A. S., & Middleton, N. J. (2006). Desert dust in the global system. Springer Science &
756 Business Media.
757 Hook, S., Hulley, G. (2022). ECOSTRESS Swath Land Surface Temperature and Emissivity
758 Instantaneous L2 Global 70 m v002 [Data set]. NASA EOSDIS Land Processes Distributed
759 Active Archive Center. Accessed 2024-04-12 from
760 https://doi.org/10.5067/ECOSTRESS/ECO_L2_LSTE.002
761 Kayet, N., Pathak, K., Chakrabarty, A., Kumar, S., Chowdary, V. M., Singh, C. P., Sahoo, S., &
762 Basumatary, S. (2019). Assessment of foliar dust using Hyperion and Landsat satellite
763 imagery for mine environmental monitoring in an open cast iron ore mining areas. Journal
764 of Cleaner Production, 218, 993–1006. https://doi.org/10.1016/j.jclepro.2019.01.305
765 Li, X., Talbot, J., King, J., & Wang, M. (2023). Effects of road dust on vegetation composition and
766 surface chemistry of three ombrotrophic peatlands in eastern Canada. Geoderma, 439,
767 116665. https://doi.org/10.1016/j.geoderma.2023.116665
768 Lin, W., Sun, Y., Wang, D., Li, Y., & Yu, X. (2021b). Estimation model of dust deposition capacity
769 of common vegetation based on spectral characteristics in Shanghai, China. Sustainable
770 Cities and Society, 70, 102915. https://doi.org/10.1016/j.scs.2021.102915
771 Lin, W., Yu, X., Xu, D., Sun, T., & Sun, Y. (2021a). Effect of Dust Deposition on Chlorophyll
772 Concentration Estimation in Urban Plants from Reflectance and Vegetation Indexes.
773 Remote Sensing, 13(18), 3570. https://doi.org/10.3390/rs13183570
774 Linden, J., Gustafsson, M., Uddling, J., Watne, Å., & Pleijel, H. (2023). Air pollution removal
775 through deposition on urban vegetation: The importance of vegetation characteristics.
776 Urban Forestry & Urban Greening, 81, 127843.
777 https://doi.org/10.1016/j.ufug.2023.127843
778 Ma, B., Li, X., Jiang, Z., Pu, R., Liang, A., & Che, D. (2020). Dust Dispersion and Its Effect on
779 Vegetation Spectra at Canopy and Pixel Scales in an Open-Pit Mining Area. Remote
780 Sensing, 12(22), 3759. https://doi.org/10.3390/rs12223759
781 Ma, B., Pu, R., Wu, L., & Zhang, S. (2017). Vegetation Index Differencing for Estimating Foliar
782 Dust in an Ultra-Low-Grade Magnetite Mining Area Using Landsat Imagery. IEEE Access, 5,
783 8825–8834. https://doi.org/10.1109/ACCESS.2017.2700474
784 Ma, H., Xiong, C., Liang, S., Zhu, Z., Song, J., Zhang, Y., & He, T. (2022). Determining the accuracy
785 of the Landsat-based land continuous variable estimator. Science of Remote Sensing, 5,
786 100054. https://doi.org/10.1016/j.srs.2022.100054
787 Mu, X., Hu, M., Song, W., Ruan, G., Ge, Y., Wang, J., Huang, S., Yan, G. (2015). Evaluation of
788 Sampling Methods for Validation of Remotely Sensed Fractional Vegetation Cover.
789 Remote Sensing. 7(12):16164-16182. https://doi.org/10.3390/rs71215817

790 Naidoo, G., & Chirkoot, D. (2004). The effects of coal dust on photosynthetic performance of
791 the mangrove, Avicennia marina in Richards Bay, South Africa. Environmental Pollution,
792 127(3), 359–366. https://doi.org/10.1016/j.envpol.2003.08.018
793 Pöschl, U. (2005). Atmospheric Aerosols: Composition, Transformation, Climate and Health
794 Effects. Angewandte Chemie International Edition, 44(46), 7520–7540.
795 https://doi.org/10.1002/anie.200501122
796 Prusty, B. A. K., Mishra, P. C., & Azeez, P. A. (2005). Dust accumulation and leaf pigment content
797 in vegetation near the national highway at Sambalpur, Orissa, India. Ecotoxicology and
798 Environmental Safety, 60(2), 228–235. https://doi.org/10.1016/j.ecoenv.2003.12.013
799 Rangwala, I., & Miller, J. R. (2012). Climate change in mountains: A review of elevation-
800 dependent warming and its possible causes. Climatic Change, 114(3–4), 527–547.
801 https://doi.org/10.1007/s10584-012-0419-3
802 Ranjan, A. K., Parida, B. R., Dash, J., & Gorai, A. K. (2023). Evaluating Impacts of Opencast Stone
803 Mining on Vegetation Primary Production and Transpiration over Rajmahal Hills.
804 Sustainability, 15(10), 8005. https://doi.org/10.3390/su15108005
805 Ranjan, A. K., Dash, J., Xiao, J., & Gorai, A. K. (2022). Vegetation activity enhanced in India
806 during the COVID-19 lockdowns: evidence from satellite data. Geocarto International,
807 37(26), 12618-12637. https://doi.org/10.1080/10106049.2022.2071469
808 Ranjan, A. K., Sahoo, D., & Gorai, A. K. (2021). Quantitative assessment of landscape
809 transformation due to coal mining activity using earth observation satellite data in
810 Jharsuguda coal mining region, Odisha, India. Environment, Development and
811 Sustainability, 23(3), 4484–4499. https://doi.org/10.1007/s10668-020-00784-0
812 Rehman, A. U., Yasmeen, K., Islam, F., Anees, S. A., Tariq, A., Zubair, M., Bilal, M., Rahman, I. U.,
813 Rahman, S. U., & Hatamleh, W. A. (2023). Assessment of heavy metal accumulation in
814 dust and leaves of Conocarpus erectus in urban areas: Implications for phytoremediation.
815 Physics and Chemistry of the Earth, Parts A/B/C, 132, 103481.
816 https://doi.org/10.1016/j.pce.2023.103481
817 Running, S., Mu, Q., Zhao, M. (2015). MOD17A2H MODIS/Terra Gross Primary Productivity 8-
818 Day L4 Global 500m SIN Grid V006 [Data set]. NASA EOSDIS Land Processes Distributed
819 Active Archive Center. Accessed 2024-04-12 from
820 https://doi.org/10.5067/MODIS/MOD17A2H.006
821 Running, S., Mu, Q., Zhao, M. (2017). MOD16A2 MODIS/Terra Net Evapotranspiration 8-Day L4
822 Global 500m SIN Grid V006 [Data set]. NASA EOSDIS Land Processes Distributed Active
823 Archive Center. Accessed 2024-04-12 from
824 https://doi.org/10.5067/MODIS/MOD16A2.006
825 Singh, A. K., Kumar, M., Bauddh, K., Singh, A., Singh, P., Madhav, S., & Shukla, S. K. (2023).
826 Environmental impacts of air pollution and its abatement by plant species: A
827 comprehensive review. Environmental Science and Pollution Research, 30(33), 79587–
828 79616. https://doi.org/10.1007/s11356-023-28164-x
829 Song, Y., Maher, B. A., Li, F., Wang, X., Sun, X., & Zhang, H. (2015). Particulate matter deposited
830 on leaf of five evergreen species in Beijing, China: Source identification and size
831 distribution. Atmospheric environment, 105, 53-60.

Su, K., Yu, Q., Hu, Y., Liu, Z., Wang, P., Zhang, Q., Zhu, J., Niu, T., & Yue, D. (2019). Inversion and Effect Research on Dust Distribution of Urban Forests in Beijing. Forests, 10(5), 418. https://doi.org/10.3390/f10050418

Subpiramaniyam, S., Boovaragamoorthy, G. M., Kaliannan, T., Krishna, K., Hong, S.-C., Yi, P.-I., Jang, S.-H., & Suh, J.-M. (2021). Assessment of foliar dust deposition and elemental concentrations in foliar dust and long rows of grand tamarind leaves along two major roads of Coimbatore, India. Chemosphere, 264, 128444. https://doi.org/10.1016/j.chemosphere.2020.128444

Sun, Y., Lin, W., Li, Y., & Xu, D. (2021). Dust deposition on vegetation leaves in Shanghai, China. International Journal of Environmental Health Research, 31(8), 1001–1014. https://doi.org/10.1080/09603123.2020.1714559

Tadono, T., Ishida, H., Oda, F., Naito, S., Minakawa, K., and Iwamoto, H. (2014).Precise Global DEM Generation by ALOS PRISM, ISPRS Annals of the Photogrammetry, Remote Sensing and Spatial Information Sciences, II-4, 71-76

Wang, H., Shi, H., Li, Y., Yu, Y., & Zhang, J. (2013). Seasonal variations in leaf capturing of particulate matter, surface wettability and micromorphology in urban tree species. Frontiers of Environmental Science & Engineering, 7, 579-588.https://doi.org/10.1007/s11783-013-0524-1

Yan, X., Shi, W., Zhao, W., & Luo, N. (2015). Mapping dustfall distribution in urban areas using remote sensing and ground spectral data. Science of The Total Environment, 506–507, 604–612. https://doi.org/10.1016/j.scitotenv.2014.11.036

Yu, H. M., Ren, G. Y., & Liu, Y. L. (2013). The characteristics of wind speed variation at different altitudes of boundary layer in Heilongjiang province. Journal of Natural Resources, 28(10), 1718–1730. (in Chinese). https://doi.org/10.11849/zrzyxb.2013.10.007

Yu, T., Wang, J., Chao, Y., & Zeng, H. (2022). Extinction Effect of Foliar Dust Retention on Urban Vegetation as Estimated by Atmospheric PM10 Concentration in Shenzhen, China. Remote Sensing, 14(20), 5103. https://doi.org/10.3390/rs14205103

Zender, C. S., Miller, R. L.R. L., Tegen, I. (2004). Quantifying mineral dust mass budgets:Terminology, constraints, and current estimates. Eos, Transactions American Geophysical Union, 85(48), 509–512. https://doi.org/10.1029/2004eo480002

Zhao, Y., Lei, S., Yang, X., Gong, C., Wang, C., Cheng, W., Li, H., & She, C. (2020). Study on Spectral Response and Estimation of Grassland Plants Dust Retention Based on Hyperspectral Data. Remote Sensing, 12(12), 2019. https://doi.org/10.3390/rs12122019

Zhou, C., Chen, S., Zhang, Y., Zhao, J., Song, D., & Liu, D. (2018). Evaluating Metal Effects on the Reflectance Spectra of Plant Leaves during Different Seasons in Post-Mining Areas, China. Remote Sensing, 10(8), 1211. https://doi.org/10.3390/rs10081211

Zhu, J., Yu, Q., Zhu, H., He, W., Xu, C., Liao, J., Zhu, Q., & Su, K. (2019). Response of dust particle pollution and construction of a leaf dust deposition prediction model based on leaf reflection spectrum characteristics. Environmental Science and Pollution Research, 26(36), 36764–36775. https://doi.org/10.1007/s11356-019-06635-4

References From the Supporting Information

Baret, F., G. Guyot, and D. J. Major. (1989). TSAVI: A Vegetation Index Which Minimizes Soil Brightness Effects On LAI And APAR Estimation. Pp. 1355–58 in 12th Canadian Symposium on Remote Sensing Geoscience and Remote Sensing Symposium, Vol. 3. Vancouver, Canada: IEEE.

Blackburn, G. A. (1998). Spectral Indices for Estimating Photosynthetic Pigment Concentrations: A Test Using Senescent Tree Leaves. International Journal of Remote Sensing 19(4):657–75. doi: 10.1080/014311698215919.

Chen, Jing M. (1996). Evaluation of Vegetation Indices and a Modified Simple Ratio for Boreal Applications. Canadian Journal of Remote Sensing 22(3):229–42. doi: 10.1080/07038992.1996.10855178.

Clevers, J. G. P. W. (1988). The application of the weighted near-infrared-red vegetation index for estimating LAI at the vegetative and generative stage of cereals. In Proc. 16th ISPRS Congr., Kyoto, Japan. Vol. 27-B7 (pp. 98-107)

Clevers, J.G.P.W., De Jong, S.M., Epema, G.F., Addink, E.A. (2000). MERIS and the Red-Edge Index. Second EARSeL Workshop on Imaging Spectroscopy, Enschede.

Crippen, R. (1990). Calculating the Vegetation Index Faster. Remote Sensing of Environment 34(1):71–73. doi: 10.1016/0034-4257(90)90085-Z.

Dash, J., and P. J. Curran. (2004). The MERIS Terrestrial Chlorophyll Index. International Journal of Remote Sensing 25(23):5403–13. doi: 10.1080/0143116042000274015.

Daughtry, C. (2000). Estimating Corn Leaf Chlorophyll Concentration from Leaf and Canopy Reflectance. Remote Sensing of Environment 74(2):229–39. doi: 10.1016/S0034-4257(00)00113-9.

Delegido, J., Verrelst, J., Alonso, L., and Moreno, J. (2011). Evaluation of Sentinel-2 Red-Edge Bands for Empirical Estimation of Green LAI and Chlorophyll Content. Sensors 11(7):7063–81. doi: 10.3390/s110707063.

Escadafal, R. (1989). Remote Sensing of Arid Soil Surface Color with Landsat Thematic Mapper. Advances in Space Research 9(1):159–63. doi: 10.1016/0273-1177(89)90481-X.

Frampton, W. J., Dash, J., Watmough, G., and James, M. E. (2013). Evaluating the Capabilities of Sentinel-2 for Quantitative Estimation of Biophysical Variables in Vegetation. ISPRS Journal of Photogrammetry and Remote Sensing 82:83–92. doi: 10.1016/j.isprsjprs.2013.04.007.

Gitelson, A. A., Kaufman, Y. J., and Merzlyak, M. N. (1996). Use of a Green Channel in Remote Sensing of Global Vegetation from EOS-MODIS. Remote Sensing of Environment 58(3):289–98. doi: 10.1016/S0034-4257(96)00072-7.

Goel, N. S., and Qin, W. (1994). Influences of Canopy Architecture on Relationships between Various Vegetation Indices and LAI and Fpar: A Computer Simulation. Remote Sensing Reviews 10(4):309–47. doi: 10.1080/02757259409532252.

Guyot, G. Baret, F. (1988). Utilisation de la haute resolution spectrale pour suivrel'etat des couverts vegetaux. In: Proceedings, 4th International Colloquium''Spectral Signatures of Objects in Remote Sensing'', Aussois, 18–22 January1988, Paris: ESA, ESA, Publication SP-287, pp. 279–286

Guyot, G., Baret, F., and Major, D. J. (1988). High spectral resolution: Determination of spectral shifts between the red and infrared. International Archives of Photogrammetry and Remote Sensing, 11, pp. 750–760.

Huete, A. R. (1988). A Soil-Adjusted Vegetation Index (SAVI). Remote Sensing of Environment 25(3):295–309. doi: 10.1016/0034-4257(88)90106-X.

Jensen, J. R. (2000). Remote sensing of the environment: An earth resource perspective. Upper Saddle River, N.J. : Prentice Hall.

Jordan, C. F. (1969). Derivation of Leaf-Area Index from Quality of Light on the Forest Floor. Ecology 50(4):663–66. doi: 10.2307/1936256.

Kaufman, Y. J., and D. Tanre. (1992). Atmospherically Resistant Vegetation Index (ARVI) for EOS-MODIS. IEEE Transactions on Geoscience and Remote Sensing 30(2):261–70. doi: 10.1109/36.134076.

Pinty, B., and M. M. Verstraete. (1992). GEMI: A Non-Linear Index to Monitor Global Vegetation from Satellites. Vegetatio 101(1):15–20. doi: 10.1007/BF00031911.

Pouget, M., Netto, J.M., Floc'h, É.L., & Kamal, S. (1991). Caractéristiques spectrales des surfaces sableuses de la région côtière Nord-Ouest de l'Egypte : application aux données satellitaires SPOT.

Qi, J., A. Chehbouni, A. R. Huete, Y. H. Kerr, and S. Sorooshian. (1994). A Modified Soil Adjusted Vegetation Index. Remote Sensing of Environment 48(2):119–26. doi: 10.1016/0034-4257(94)90134-1.

Richardsons, A.J., & Wiegand, A. (1977). DISTINGUISHING VEGETATION FROM SOIL BACKGROUND INFORMATION. Photogrammetric Engineering and Remote Sensing, 43, 1541-1552.

Rouse, J.W., Haas, R.H., Schell, J.A., Deering, W.D., (1973). Monitoring vegetation systems in the Great Plains with ERTS. In: Third ERTS Symposium, NASA SP-351,pp. 309–317.

Senseman, G.M., Tweddale, S.A., Anderson, A.B., & Bagley, C.F. 1996. Correlation of Land Condition Trend Analysis (LCTA) Rangeland Cover Measures to Satellite-Imagery-Derived Vegetation
Indices.http://www.cecer.army.mil/techreports/and_vegi/AND_VEGI.LLN.post.PDF

Figure 1.

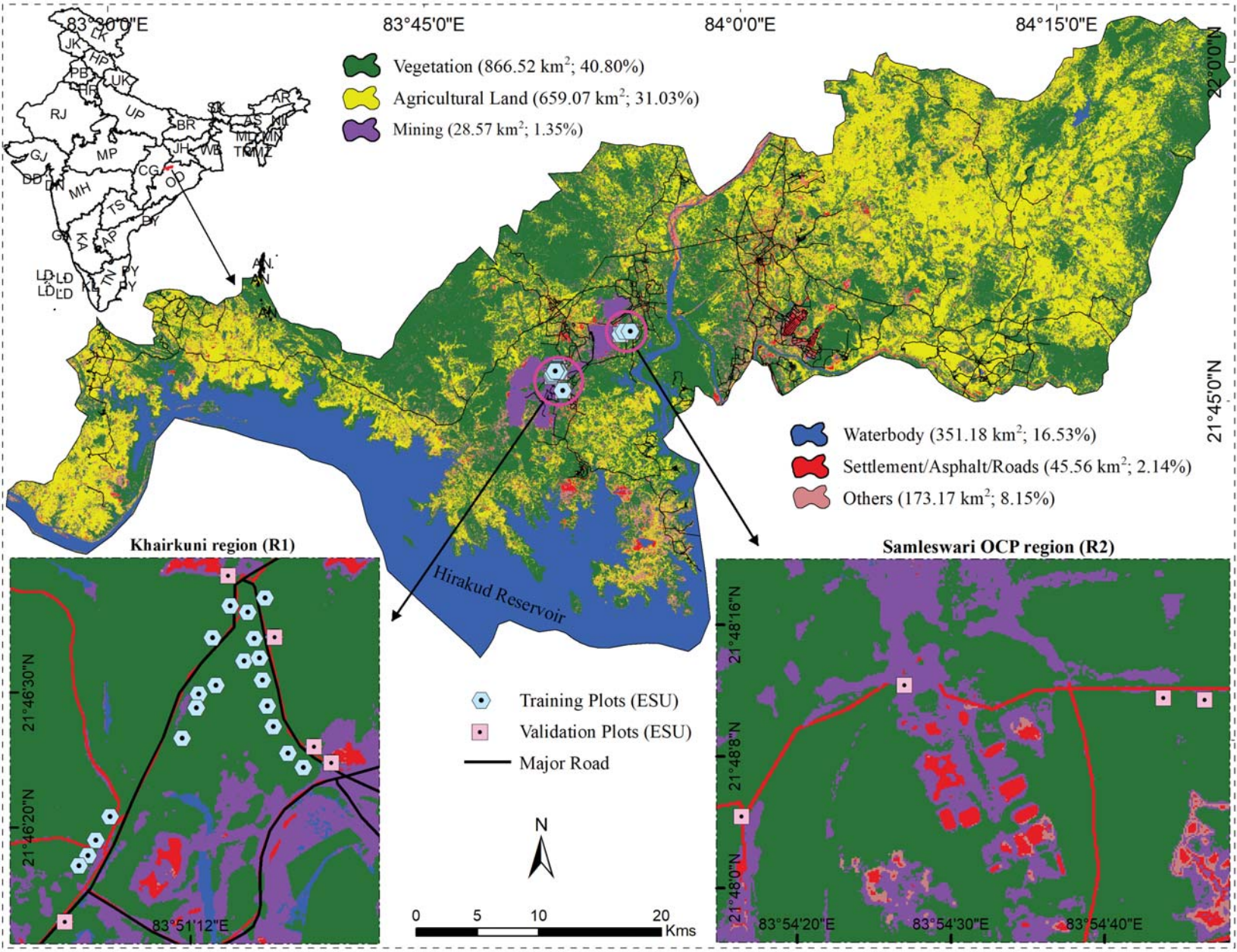
83°30'0"E
83°45'0"E
84°0'0"E
84°15'0"E
22°0'0"N
21°45'0"N
Vegetation (866.52 km2; 40.80%)
Agricultural Land (659.07 km2; 31.03%)
Mining (28.57 km2; 1.35%)
Waterbody (351.18 km2; 16.53%)
Settlement/Asphalt/Roads (45.56 km2; 2.14%)
Others (173.17 km2; 8.15%)
Hirakud Reservoir
Khairkuni region (R1)
Samleswari OCP region (R2)
21°46'30"N
21°46'20"N
83°51'12"E
21°48'16"N
21°48'8"N
21°48'0"N
83°54'20"E
83°54'30"E
83°54'40"E
Training Plots (ESU)
Validation Plots (ESU)
Major Road
N
0 5 10 20
Kms

Figure 2.

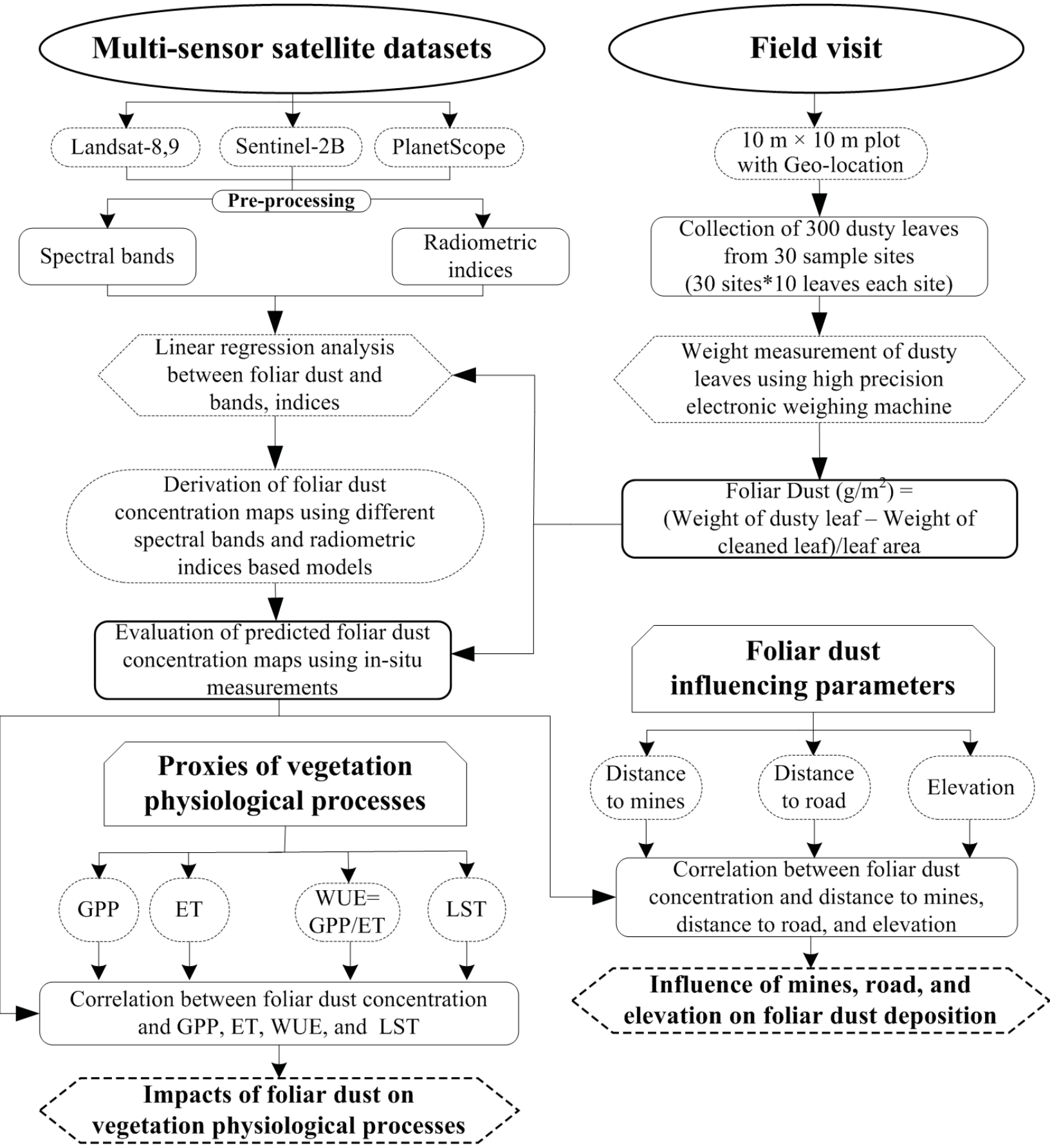
Multi-sensor satellite datasets
Field visit
Landsat-8,9
Sentinel-2B
PlanetScope
Pre-processing
Spectral bands
Radiometric indices
10 m × 10 m plot with Geo-location
Collection of 300 dusty leaves from 30 sample sites (30 sites*10 leaves each site)
Linear regression analysis between foliar dust and bands, indices
Weight measurement of dusty leaves using high precision electronic weighing machine
Derivation of foliar dust concentration maps using different spectral bands and radiometric indices based models
Foliar Dust (g/m2) = (Weight of dusty leaf – Weight of cleaned leaf)/leaf area
Evaluation of predicted foliar dust concentration maps using in-situ measurements
Foliar dust influencing parameters
Proxies of vegetation physiological processes
Distance to mines
Distance to road
Elevation
GPP
ET
WUE= GPP/ET
LST
Correlation between foliar dust concentration and distance to mines, distance to road, and elevation
Correlation between foliar dust concentration and GPP, ET, WUE, and LST
Influence of mines, road, and elevation on foliar dust deposition
Impacts of foliar dust on vegetation physiological processes

Figure 3.

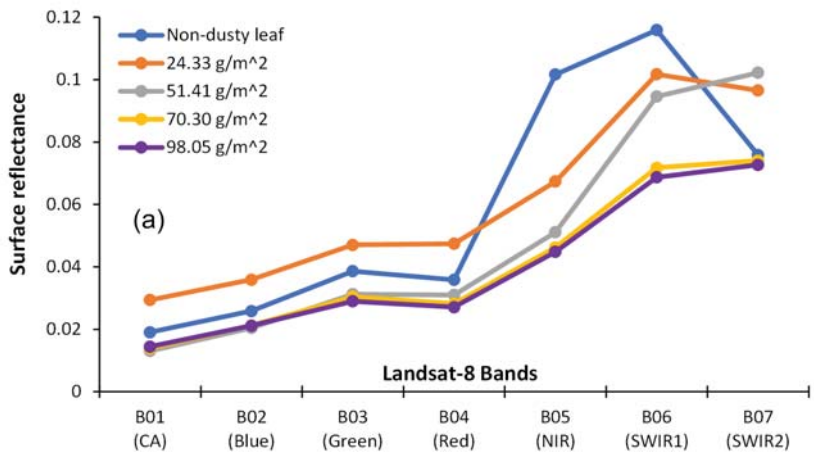
Non-dusty leaf
24.33 g/m^2
51.41 g/m^2
70.30 g/m^2
98.05 g/m^2
(a)
Surface reflectance
0.12
0.1
0.08
0.06
0.04
0.02
0
Landsat-8 Bands
B01 (CA)
B02 (Blue)
B03 (Green)
B04 (Red)
B05 (NIR)
B06 (SWIR1)
B07 (SWIR2)

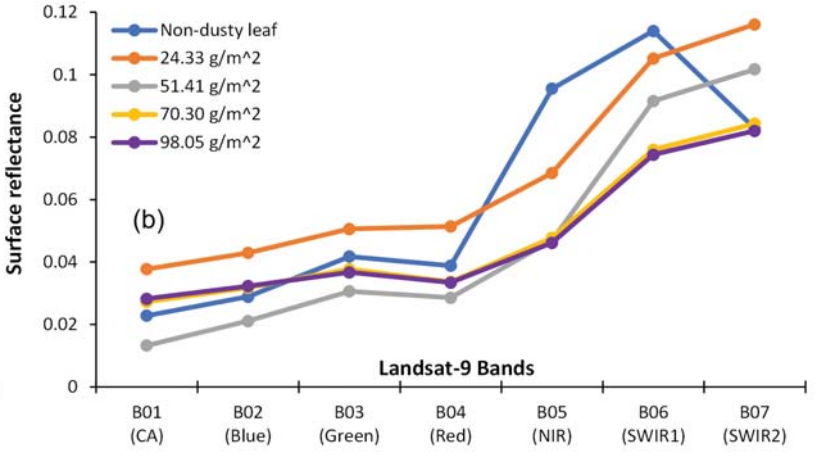
Non-dusty leaf
24.33 g/m^2
51.41 g/m^2
70.30 g/m^2
98.05 g/m^2
(b)
Surface reflectance
0.12
0.1
0.08
0.06
0.04
0.02
0
Landsat-9 Bands
B01 (CA)
B02 (Blue)
B03 (Green)
B04 (Red)
B05 (NIR)
B06 (SWIR1)
B07 (SWIR2)

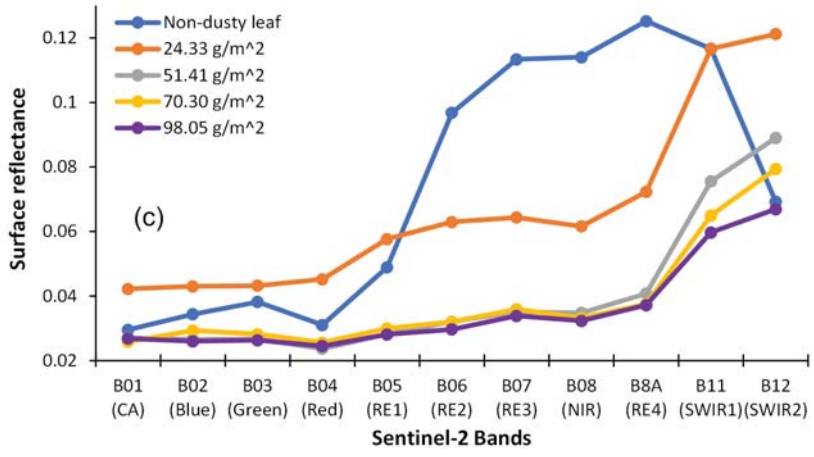
Non-dusty leaf
24.33 g/m^2
51.41 g/m^2
70.30 g/m^2
98.05 g/m^2
(c)
Surface reflectance
0.12
0.1
0.08
0.06
0.04
0.02
Sentinel-2 Bands
B01 (CA)
B02 (Blue)
B03 (Green)
B04 (Red)
B05 (RE1)
B06 (RE2)
B07 (RE3)
B08 (NIR)
B8A (RE4)
B11 (SWIR1)
B12 (SWIR2)

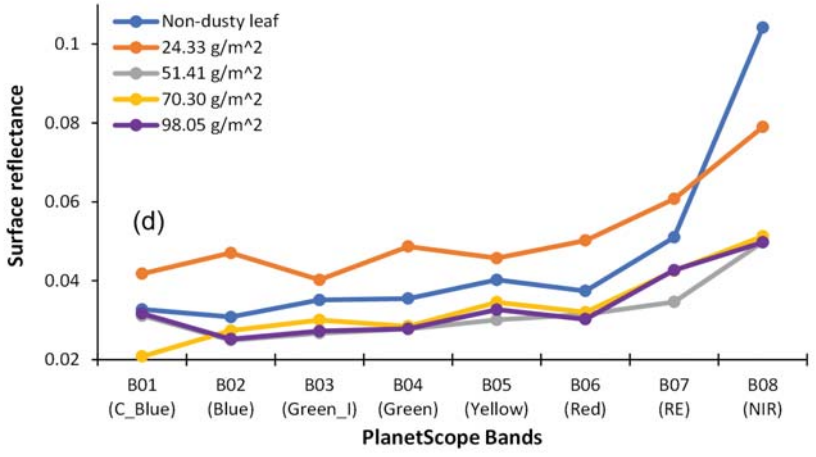
Non-dusty leaf
24.33 g/m^2
51.41 g/m^2
70.30 g/m^2
98.05 g/m^2
(d)
Surface reflectance
0.1
0.08
0.06
0.04
0.02
PlanetScope Bands
B01 (C_Blue)
B02 (Blue)
B03 (Green_I)
B04 (Green)
B05 (Yellow)
B06 (Red)
B07 (RE)
B08 (NIR)

Figure 4.

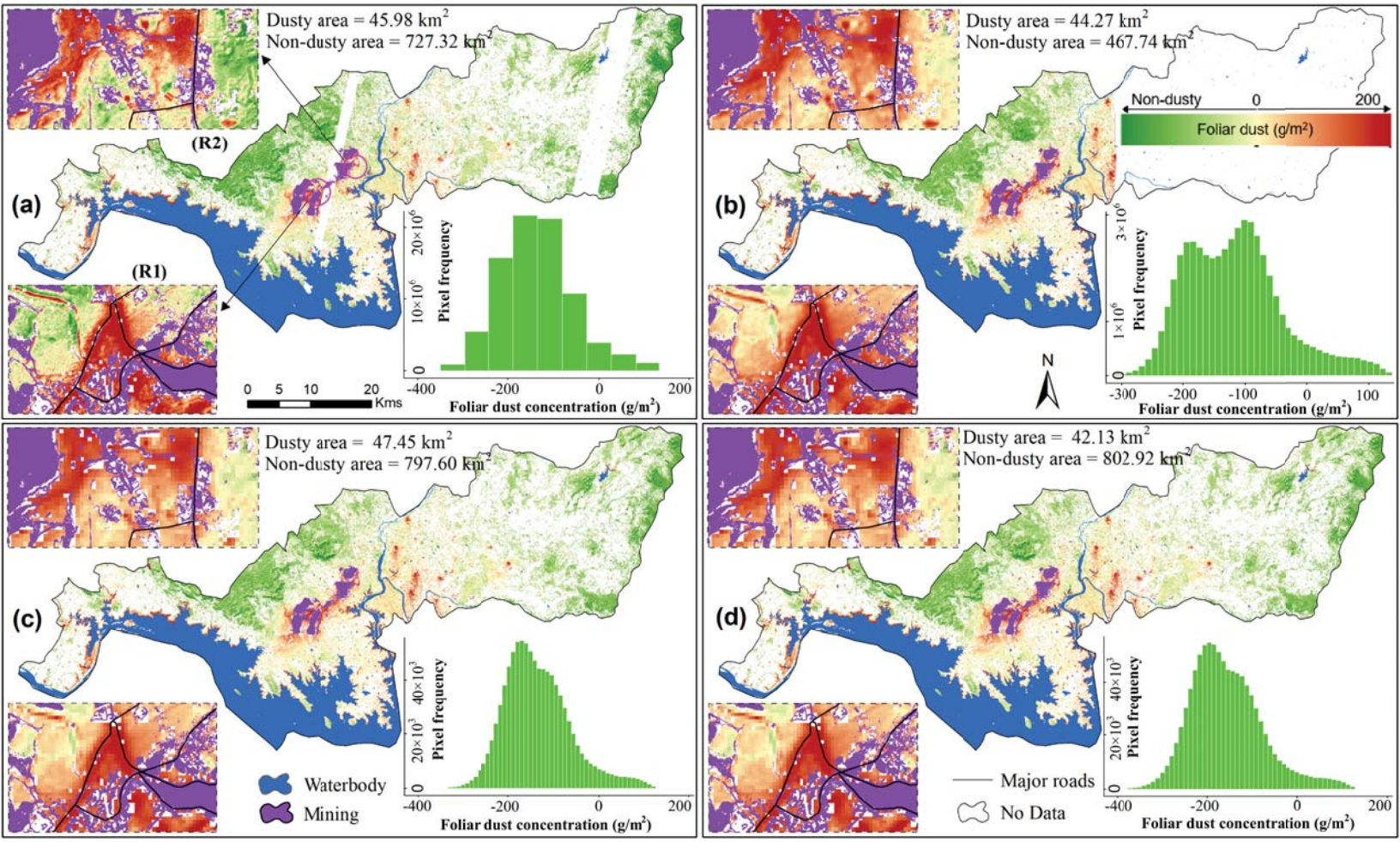
(a)
Dusty area = 45.98 km²
Non-dusty area = 727.32 km²
(R2)
(R1)
0 5 10 20 Kms
Pixel frequency
0
10×10⁶
20×10⁶
-400 -200 0 200
Foliar dust concentration (g/m²)
(b)
Dusty area = 44.27 km²
Non-dusty area = 467.74 km²
Non-dusty 0 200
Foliar dust (g/m²)
N
Pixel frequency
0
1×10⁶
3×10⁶
-300 -200 -100 0 100
Foliar dust concentration (g/m²)
(c)
Dusty area = 47.45 km²
Non-dusty area = 797.60 km²
Waterbody
Mining
Pixel frequency
0
20×10³
40×10³
-400 -200 0 200
Foliar dust concentration (g/m²)
(d)
Dusty area = 42.13 km²
Non-dusty area = 802.92 km²
Major roads
No Data
Pixel frequency
0
20×10³
40×10³
-400 -200 0 200
Foliar dust concentration (g/m²)

Figure 5.

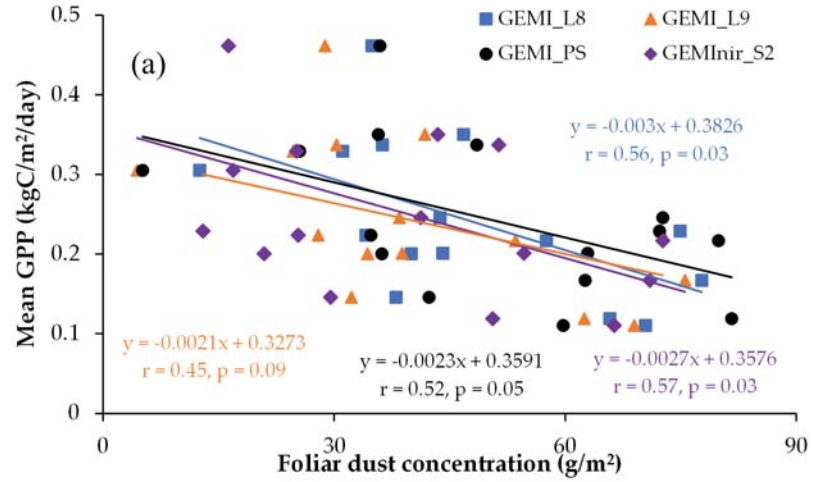
(a)
GEMI_L8
GEMI_L9
GEMI_PS
GEMInir_S2
y = -0.003x + 0.3826
r = 0.56, p = 0.03
y = -0.0021x + 0.3273
r = 0.45, p = 0.09
y = -0.0023x + 0.3591
r = 0.52, p = 0.05
y = -0.0027x + 0.3576
r = 0.57, p = 0.03
Mean GPP (kgC/m²/day)
Foliar dust concentration (g/m²)

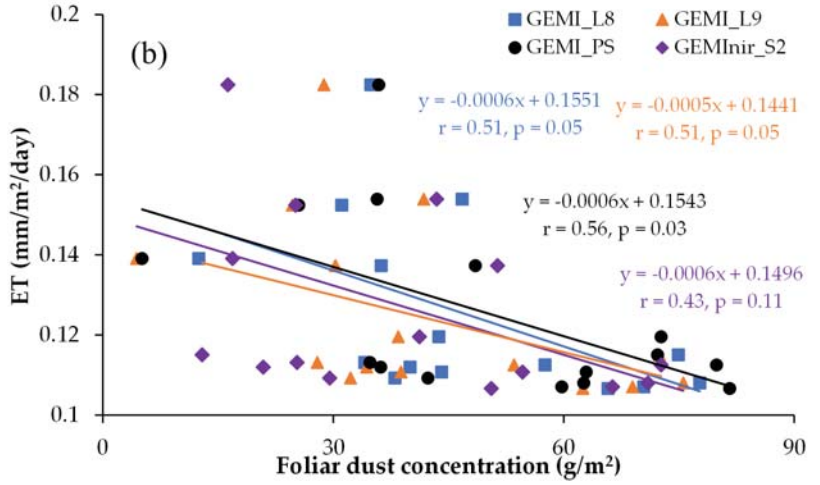
(b)
GEMI_L8
GEMI_L9
GEMI_PS
GEMInir_S2
y = -0.0006x + 0.1551
r = 0.51, p = 0.05
y = -0.0005x + 0.1441
r = 0.51, p = 0.05
y = -0.0006x + 0.1543
r = 0.56, p = 0.03
y = -0.0006x + 0.1496
r = 0.43, p = 0.11
ET (mm/m²/day)
Foliar dust concentration (g/m²)

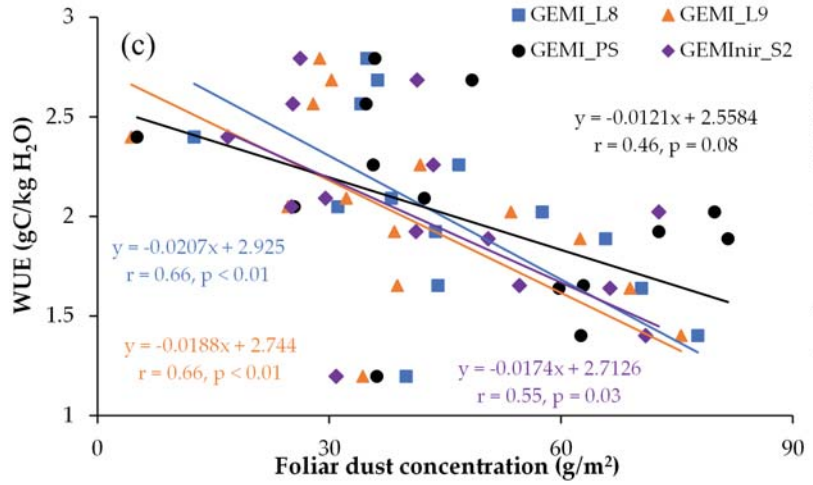
(c)
GEMI_L8
GEMI_L9
GEMI_PS
GEMInir_S2
y = -0.0121x + 2.5584
r = 0.46, p = 0.08
y = -0.0207x + 2.925
r = 0.66, p < 0.01
y = -0.0188x + 2.744
r = 0.66, p < 0.01
y = -0.0174x + 2.7126
r = 0.55, p = 0.03
WUE (gC/kg H2O)
Foliar dust concentration (g/m²)

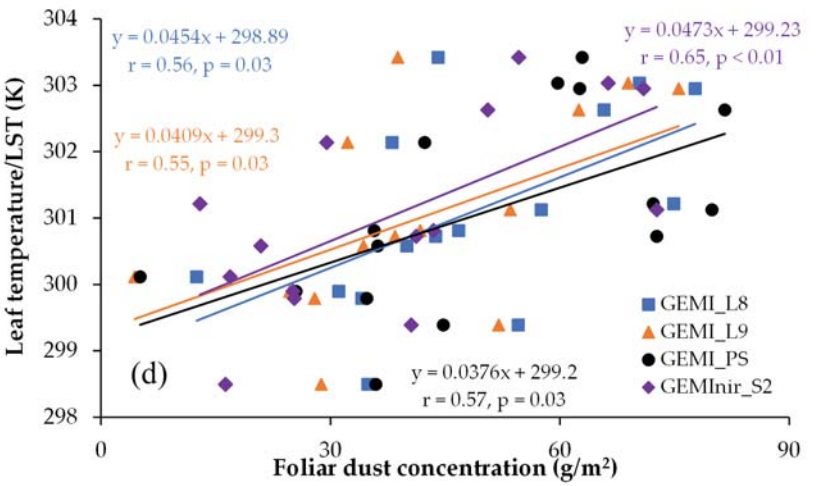
(d)
y = 0.0454x + 298.89
r = 0.56, p = 0.03
y = 0.0473x + 299.23
r = 0.65, p < 0.01
y = 0.0409x + 299.3
r = 0.55, p = 0.03
y = 0.0376x + 299.2
r = 0.57, p = 0.03
GEMI_L8
GEMI_L9
GEMI_PS
GEMInir_S2
Leaf temperature/LST (K)
Foliar dust concentration (g/m²)

Figure 6.

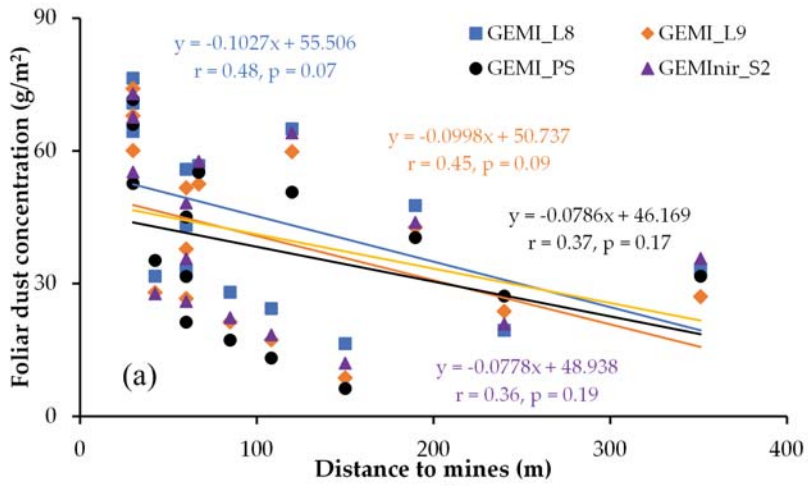
GEMI_L8
GEMI_L9
GEMI_PS
GEMInir_S2
y = -0.1027x + 55.506
r = 0.48, p = 0.07
y = -0.0998x + 50.737
r = 0.45, p = 0.09
y = -0.0786x + 46.169
r = 0.37, p = 0.17
y = -0.0778x + 48.938
r = 0.36, p = 0.19
(a)
Foliar dust concentration (g/m²)
Distance to mines (m)
0
30
60
90
0
100
200
300
400

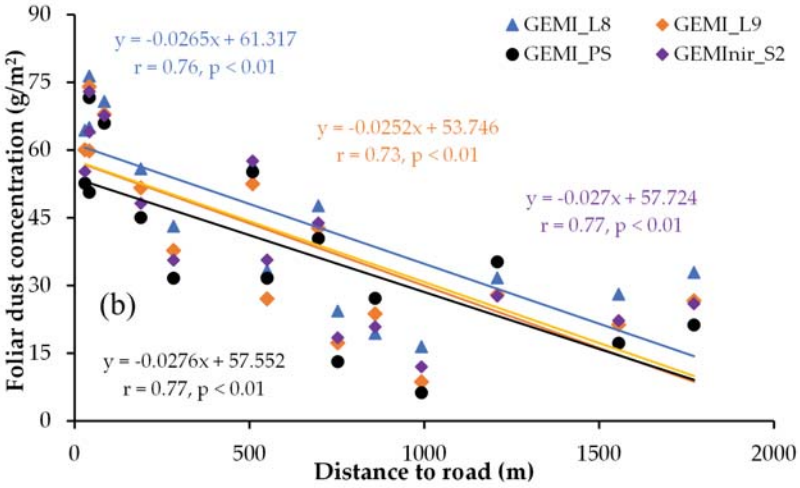
GEMI_L8
GEMI_L9
GEMI_PS
GEMInir_S2
y = -0.0265x + 61.317
r = 0.76, p < 0.01
y = -0.0252x + 53.746
r = 0.73, p < 0.01
y = -0.027x + 57.724
r = 0.77, p < 0.01
y = -0.0276x + 57.552
r = 0.77, p < 0.01
(b)
Foliar dust concentration (g/m²)
Distance to road (m)
0
15
30
45
60
75
90
0
500
1000
1500
2000

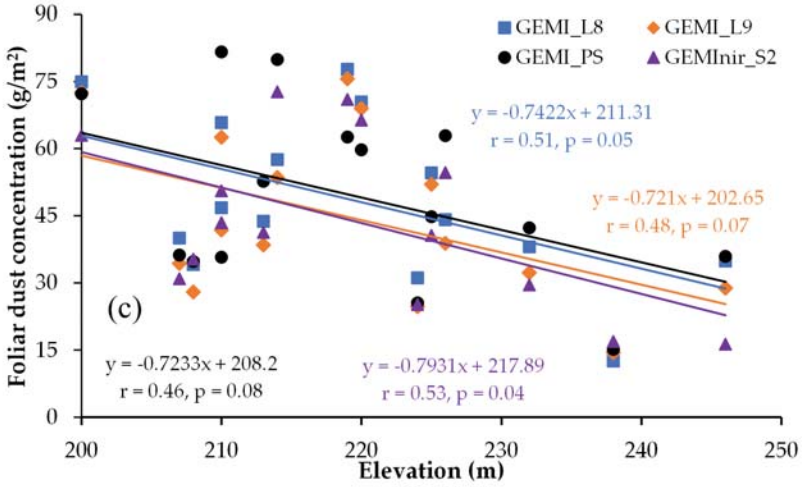
GEMI_L8
GEMI_L9
GEMI_PS
GEMInir_S2
y = -0.7422x + 211.31
r = 0.51, p = 0.05
y = -0.721x + 202.65
r = 0.48, p = 0.07
y = -0.7233x + 208.2
r = 0.46, p = 0.08
y = -0.7931x + 217.89
r = 0.53, p = 0.04
(c)
Foliar dust concentration (g/m²)
Elevation (m)
0
15
30
45
60
75
90
200
210
220
230
240
250